ESBO DS
Stratospheric Observatory

D4.1 – ESBO DS DESIGN JUSTIFICATION FILE

Version 1.0

04.01.2021

Status: Released

European Commission

Deliverable

H2020 INFRADEV-01-2017 project "European Stratospheric Balloon Observatory *Design Study*"

Topic: INFRADEV-01-2017 Design Studies

Project Title: European Stratospheric Balloon Observatory *Design Study* – ESBO *DS*

Proposal No: 777516 – ESBO DS

Duration: Mar 1, 2018 - Feb 28, 2021

WP	4
Del. No	D4.1
Title	ESBO *DS* Design Justification File
Lead Beneficiary	"USTUTT"
Nature	"Report"
Dissemination Level	"Public"
Est. Del. Date	30/04/2019
Version	1.0
Date	04.01.2021
Status	Released
Authors	ESBO *DS* Team
Approved by	ESBO *DS* Team

TABLE OF CONTENTS

LIST OF ABBREVIATIONS AND DEFINITIONS

Abbreviation	Definition
Avg.	Average
BLOS	Beyond line of sight
CBE	Current Best Estimate
CEST	Central European Summer Time
CFRP	Carbon Fibre Reinforced Polymer
CTE	Coefficient of Thermal Expansion
Dec.	Declination
EDT	Eastern Daylight Time
Elev.	Elevation
ESBO	European Stratospheric Balloon Observatory
FIR	Far Infrared
HALOE	Halogen Occultation Experiment
LDB	Long Duration Ballooning
LOS	Line of sight
Max.	Maximum
MCF	Million Cubic Feet
Min.	Minimum
MODTRAN	Moderate Resolution Atmospheric Transmission
NIR	Near Infrared
NZ	New Zealand
NZDT	New Zealand Daylight Time
NZST	New Zealand Standard Time
OMI	Ozone Monitoring Instrument
OTA	Optical tube assembly
PWV	Precipitable Water Vapour
RA	Right Ascension
sCMOS	scientific Complementary metal-oxide-semiconductor
SiC	Silicon Carbide

SOFIA	Stratospheric Observatory for Infrared Astronomy
SPB	Super Pressure Balloon
STUDIO	Stratospheric Ultraviolet Demonstrator of an Imaging Observatory
ULDB	Ultra Long Duration Ballooning
TBC	To be confirmed
TBD	To be determined
UARS	Upper Atmosphere Research Satellite
UT	Universal Time
UV	Ultraviolet
YSO	Young Stellar Object
ZPB	Zero Pressure Balloon

REFERENCE DOCUMENTS

[RD1]	Hibbits, C., Bauer, J., Bernasconi, P., Clarke, J., Domingue, D., Emery, J., Gladstone, R., Greathouse, T., Hansen, G., Harris, W., Hendrix, A., Izenberg, N., Lisse, C., Paxton, L., Percival, J., Retherford, K., Rivkin, A., Swain, M., Young, E., Stratospheric Balloon Missions for Planetary Science: A Petition for the Formation of a Working Group to Study the Feasibility of a Facility Platform to Support Planetary Science Missions.
[RD2]	Young, E., Hibbitts, C., Emery, J., Hendrix, A., Merline, W., Grundy, W., Retherford, K., Balloon-Borne Telescopes for Planetary Science: Imaging and Photometry, White Paper.
[RD3]	Lemke, D., Frey, A., Haussecker, K., Hofmann, W., Salm, N., Schütz, H., Ballonteleskop THISBE 1 – Technik, Ergebnisse, Erfahrungen, Research Report, 1976 (in German).
[RD4]	Borden, M., Lewis, D., Ochoa, H., Jones-Wilson, L., Susca, S., Porter, M., … Netterfield, B. (2017). Thermal, structural, and optical analysis of a balloon-based imaging system. *Publications of the Astronomical Society of the Pacific*, *129*(973), 1–31. https://doi.org/10.1088/1538-3873/129/973/035001
[RD5]	Soler, J. D., Ade, P. A. R., Angilè, F. E., Benton, S. J., Devlin, M. J., Dober, B., … Ward-Thompson, D. (2014). Thermal design and performance of the balloon-borne large aperture submillimeter telescope for polarimetry BLASTPol. *Proceedings of SPIE - The International Society for Optical Engineering*, *9145*. https://doi.org/10.1117/12.2055431
[RD6]	Bicak, Ibrahim. Investigation of wind conditions, viewing conditions, and potential flight trajectories of balloon-based telescopes over Antarctica. Bachelor Thesis. Stuttgart, 2019.

[RD7]	Yoshihiro Tomikawa, Kaoru Sato, Naohiko Hirasawa, Masaki Tsutsumi, and Takuji Nakamura. Balloon-borne observations of lower stratospheric water vapor at Syowa station, Antarctica in 2013. Polar Science, 9(4):345{353, 2015.
[RD8]	Rosenlof, K. Distribution of water vapour in the stratosphere. Lecture at the Cargèse International School *Water vapour in the Climate System*. 14-26 September 2009.
[RD9]	Lord, S. D., 1992, NASA Technical Memorandum 103957.
[RD10]	ESBO *DS*. FIR Atmospheric Transmission Analysis. Technical Note.
[RD11]	ESBO *DS*. D2.1-2 Requirements Baseline - NIR and FIR. Version 1.0. 31 May 2018.
[RD12]	ESBO *DS*. D3.2 Concepts Preliminary Technical Specification. Version 1.0 30 April 2019.
[RD13]	ESBO *DS*. STUDIO Sky Accessibility. Version 1.02. Technical Note. 05 December 2018.
[RD14]	Fairbrother, D. Scientific Balloon Missions of Opportunity. Presentation. 16.09.2016.
[RD15]	Wertz et al. 2011, Space Mission Engineering. Microcosm Press, Hawthorne, USA.
[RD16]	ORISON. State of the Art and Market Offer Report. Version 1.1. 12 September 2017.
[RD17]	ORISON. Feasibility Report. Version 1.2. 26 September 2017.
[RD18]	ARIEL Team. ARIEL Assessment Study Report. ESA/SCI(2017)2. March 2017.
[RD19]	Columbia Scientific Balloon Facility. Structural Requirements and Recommendations for Balloon Gondola Design. Technical Report OM-220-10-H Rev. A, National Aeronautics and Space Administration, 23 April 2013.
[RD20]	ESBO *DS*. D4.4 Prototype Requirements Document. Version 1.0. 31 March 2019.

1 INTRODUCTION

This document contains technical background information on the infrastructure design concepts as described in the Preliminary Technical Specification [RD12] as well as details on the concept choice. It particularly serves to present information necessary to justify the major design choices.

Chapter 3 thereby shortly summarizes the main elements of the chosen concept. The following chapters then provide background on the choices taken and on the technical estimates made so far. Chapter 4 thereby provides justification on major requirement definitions. Chapter 5 covers technical background on the potential performance of Super Pressure Balloons. This chapter also serves to present the available observation times & accessible areas of the sky on different flight routes. In Chapter 6, details on the dimensioning of the most critical subsystems are presented. Chapter 7 eventually provides details on major trade-offs that were undertaken for the individual concepts.

2 SCOPE

This document provides a brief overview of the technical infrastructure concept chosen for further analysis. It furthermore focuses mostly on the technical justification of aspects of the mid- and long-term flight platforms envisioned for ESBO. Details on the UV/VIS flight platform, which to a large extend coincides with the prototype mission STUDIO (Stratospheric UV Demonstrator of an Imaging Observatory), will be mostly presented in the Prototype Design Definition File (D11.2).

Subsystem requirements resulting from the concept choice are included in more detail in the Technical Specification Documents (D4.2), a first list of foreseen interfaces is established in D4.3. In addition, the "Technology Demonstration" requirements for the prototype as well as further development needs are summarized in the Prototype Requirements Document (D4.4).

This document does not cover all aspects (i.e. all requirements and all subsystems) of the concepts, but focuses on design drivers and most critical aspects. Its degree of technical detail is in line with the early design stage of the concepts. More in-depth designs & analyses, based on the conclusions of the work done in Work Packages 3 and 4, will be undertaken (and documented) within Work Package 5.

3 SUMMARY OF CONCEPT FOR FURTHER ANALYSIS

This chapter shortly outlines the technical concept chosen for further analysis under Work Package 5, based on the preliminary description and the trade-offs as included in [RD12].

3.1 GENERAL OPERATIONAL CONCEPT[1]

Flight platforms are designed so that they can be flown (with minor adjustments) on different flight routes[2], with the following baseline flight routes:

[1] Further details on suitable governance infrastructure, potential ownership of equipment, etc. will be analyzed under WP6 and documented in the Operations and Governance Report.

[2] Compare see trade-off ESBO-FP-TO-01

- UV/vis flight system: circumglobal at mid-latitudes[3], flight altitude ≥ 38 km
- NIR flight system: circumglobal at mid-latitudes, flight altitude ≥ 38 km
- FIR flight system: circumpolar, Antarctica, flight altitude 25 to 30 km

3.2 FLIGHT SYSTEMS

Given the considerable differences in requirements stemming from the instruments and observations, we currently assume that dedicated gondolas are required for each of the three considered flight systems. Nevertheless, we do expect that it will be possible to use common systems / easily scale at least the following subsystems (either by using more or less modules or by exchanging only part of the system):

- Power System
- Gondola Control & Communication System
- Ballast System
- Parachute System
- Payload computing, data handling, and support
- (Thermal Control System)

We will be able to judge the scalability better after further assessment under WP5. Systems for which we expect major new designs to be necessary are particularly the gondola structure (for the FIR system), the attitude control system (for the FIR system), the balloon (for the FIR system), and large parts of the thermal control system.

3.2.1 UV/VIS Flight System

The UV/vis flight platform is to be designed to carry 0.5 m aperture class telescopes with the instruments bench directly attached to the telescope. It will thereby allow a total mass of the elevation controlled payload (telescope + instruments bench) of up to 200 kg. In order to offer maximum flexibility, it will be designed to allow an exchange of the entire telescope, of the instruments bench attached to the telescope backplate (up to approx. 600 mm diameter and 45 kg mass), and of individual instruments on the bench, with a maximum mass of approx. 6 kg. [4]

The baseline telescope chosen is a closed-tube design that allows protection of all optical elements against dust during ascent (particularly important for observations at short wavelengths)[5] and without inherent image stabilization (which would have required a secondary mirror actuated at high frequencies and posing significant structural challenges)[6]. Image stabilization, as part of a 2-stage pointing system, is rather provided by an actuated mirror in the converging beam on the instruments bench. As the sensor of the image stabilization system, a commercial sCMOS camera will be used.[7] This inner and the outer stage of the pointing system are baselined to work independently of each other.

[3] Prototype test flight & first science considered under summer/autumn turnaround conditions in Kiruna or Timmins

[4] See trade-off PL-TO-01 (all numbered trade-offs refer to [RD12])

[5] See trade-off PL-TO-04

[6] See trade-off PL-TO-02

[7] See trade-off PL-TO-07

In order to allow long duration flights, the flight platform will be equipped with both line-of-sight (LOS) and beyond-line-of-sight (BLOS) communication systems, as well as with solar arrays and secondary batteries for long-term power supply.

3.2.2 NIR Flight System

The NIR flight platform is to be designed to carry 1 m aperture class passively cooled telescopes with the instruments bench directly attached to the telescope, i.e. in an equivalent layout to the UV/vis flight platform. It shall allow a total elevation controlled mass (telescope + instruments bench) of up to approx. 700 kg, supporting instrument bench of up to approx. 400 kg. As payload interfaces, the exchangeability of both the full telescope or the instruments bench is foreseen.

As the UV/vis flight system, the NIR concept foresees a 2-stage pointing system. Given the foreseen observations during daytime (as opposed to the UV/vis platform), the NIR flight system foresees fully performant daytime-capability of the pointing system.

As for the UV/vis system, the NIR platform foresees solar arrays and secondary batteries for power supply and both LOS and BLOS communication (with the BLOS communication link being the baseline for science downlink given that only very short passes over potential ground stations are expected on the mid-latitude flight route).

Using the same architecture as the UV/vis platform, it is expected that the same modular structure approach can be used as well as most parts of the attitude control system.

3.2.3 FIR Flight System

The FIR flight platform is designed to carry a 5 m class, passively cooled telescope, baselined with a circular aperture. The platform will be designed to support a total telescope mass (including mirrors, structure, and mounting structure) of up to approx. 800 kg. Instruments are foreseen to be installed in an instrument bay, not elevation controlled, supporting up to approx. 300 kg instruments (including cryostat / instrument coolers / etc.). Given the system size and complexity, only the exchange of instruments is foreseen.

As the NIR platform, the FIR platform foresees a fully daytime-compatible two-stage pointing system and solar arrays for long-term power supply. Given the baselined Antarctic flight route, the main science data downlink is foreseen via an LOS system, while a BLOS system is carried for intermediate communication and downlink between ground station passes.

4 JUSTIFICATION OF TOP-LEVEL TECHNICAL REQUIREMENTS

This chapter presents the justification for the derivation of major top-level technical requirements from the scientific user needs and requirements as documented in the Requirements Baseline [RD11]. This particularly concerns the mission-defining requirements on flight altitude and on tolerable sky background (i.e. day vs. night time observations.

4.1 UV

UV observations of faint astronomical targets, as they are foreseen under ESBO *DS*, are still comparatively sensitive to details of the environmental conditions due to two main reasons: UV light suffers from absorption by atmospheric ozone (O_3), which is still found at high

altitudes; at the short UV wavelengths, Rayleigh scattering in the atmosphere is highly efficient, which leads to high background contributions from scattered sunlight. The next sections will investigate these effects in more detail and draw conclusions on preferable or necessary mission element implementations.

Promising launch sites for UV observations, as also mentioned in [RD12], are mainly Esrange (close to Kiruna, Sweden), Timmins (Canada), Alice Springs (Australia), and potentially in the future, for ultra long duration flights, Wanaka (New Zealand). Suitable flight times for the first three are during local turnaround conditions of the high stratospheric winds, when flight routes covering up to approx. 2 days flight in close proximity to the launch location are possible. The launch sites and preferable launch windows are summarized in Table 1.

Table 1: Suitable launch locations for UV observation flights

Launch site	**Coordinates**	**Launch windows**	**Type of flight**
Esrange, Sweden	67°53' N 21°06' E	- late April / early May - second half of August	Turnaround
Timmins, Canada	48°28' N 81°20' W	- early / late May - September	Turnaround
Alice Springs, Australia	23°42' S 133°48' E	- first half of April - second half of October	Turnaround
Wanaka, New Zealand[8]	*44°43' S* *169° 15' E*	25 March – 08 September	*Circumglobal (ULDB)*

For the analyses in sections 4.1.1 and 4.1.2, Kiruna was used as a reference location.

4.1.1 Requirements on Flight Altitude

Estimates of atmospheric transmission over the UV spectral range under possible flight conditions (launch from Kiruna) were carried out for different altitudes (ranging from 30 km to 40 km) and different zenith angles (depending on the location of the target on sky, ranging from 30° to 90° (with 90° corresponding an observation on the horizon; observations closer than 30° to the zenith are blocked by the balloon)). Simulations were carried out with the radiative transfer code MODTRAN4. Several limitations apply to the simulations:

- A built-in model atmosphere was used that is not specific for or based on atmospheric measurements from the launch sites.
- The atmospheric model used is rather old (2000), however some parameters (total ozone and water vapour columns, CO_2 mixing ratio) were adjusted to more recent (2013) numbers.
- The atmospheric model was not chosen based on actual location (latitude) and time of year, but based on the fit of simulation results to MODTRAN6 simulations for the actual latitude range and time of year. MODTRAN4 results for high latitudes and

[8] Potential future option with ULDB flights

winter showed better transmission than MODTRAN6 results for the same conditions. The results shown here are thus likely conservative estimates.

To obtain a better impression, more detailed calculations with an atmospheric model based on more recent atmospheric measurements in Kiruna can be carried out.

Figure 1 to Figure 4 show the results of the transmittance simulations over the spectral range from 200 to 600 nm, with the relevant range for the regarded UV observations being 180 nm to 330 nm (unfortunately, MODTRAN4 does not allow simulations below 200 nm).

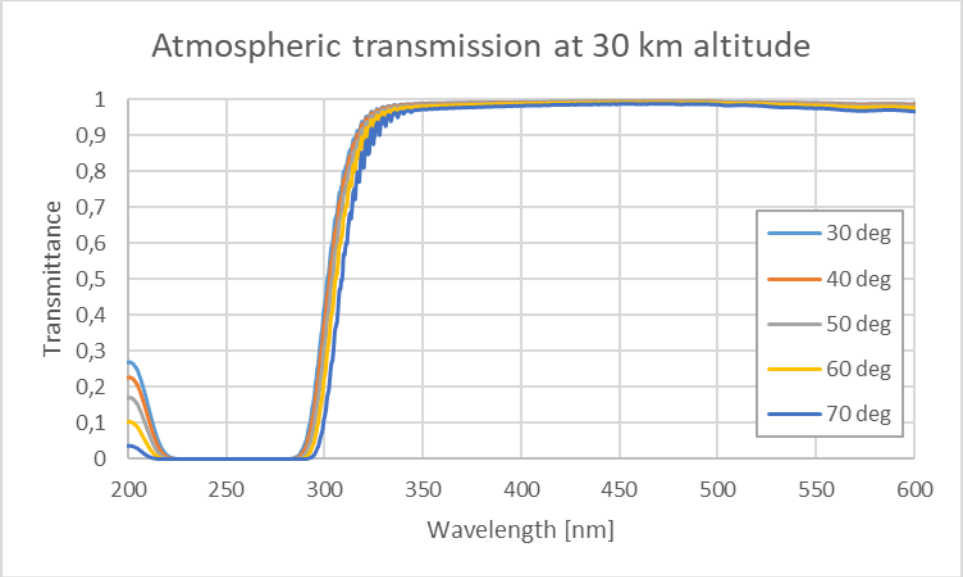

Figure 1: MODTRAN4 results for transmission at 30 km altitude

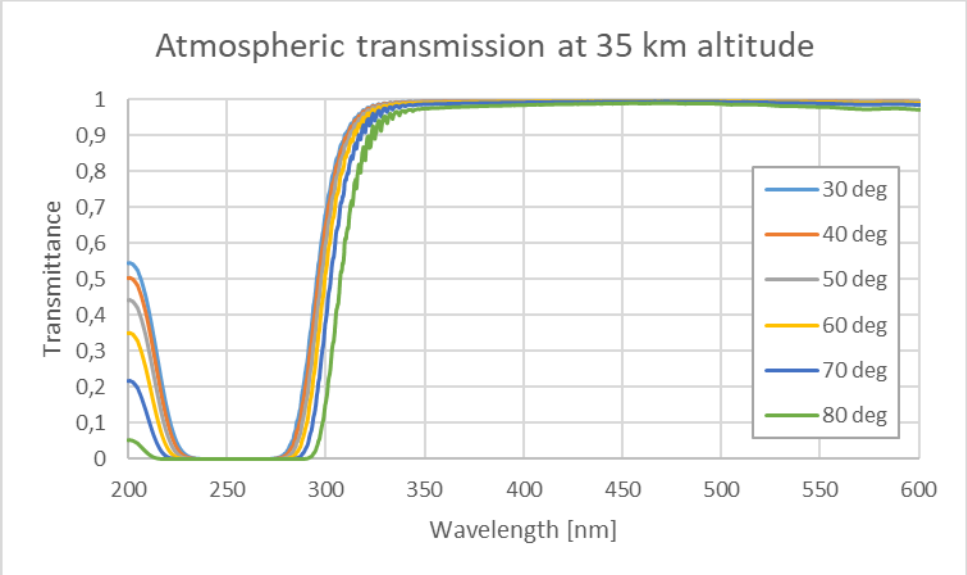

Figure 2: MODTRAN4 results for transmission at 35 km altitude

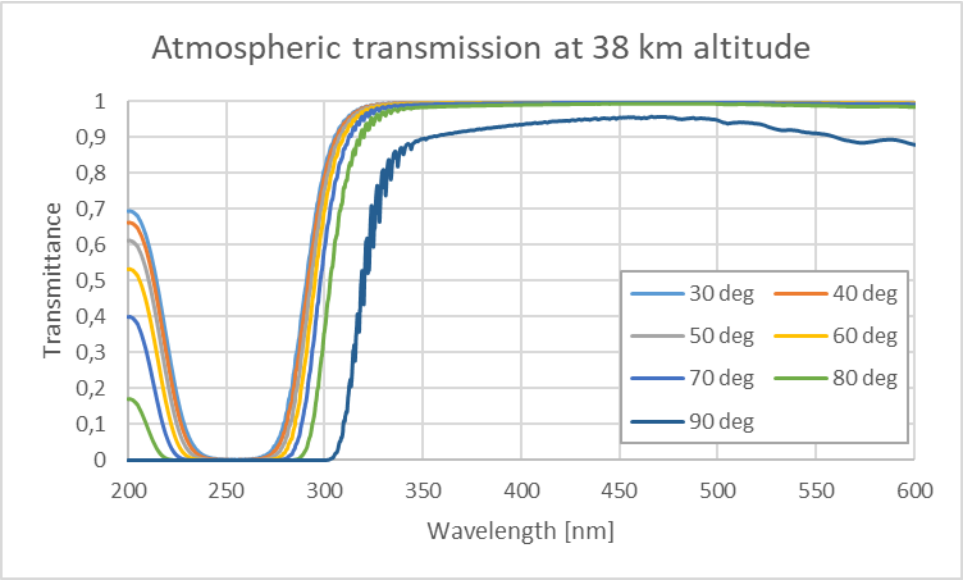

Figure 3: MODTRAN4 results for transmission at 38 km altitude

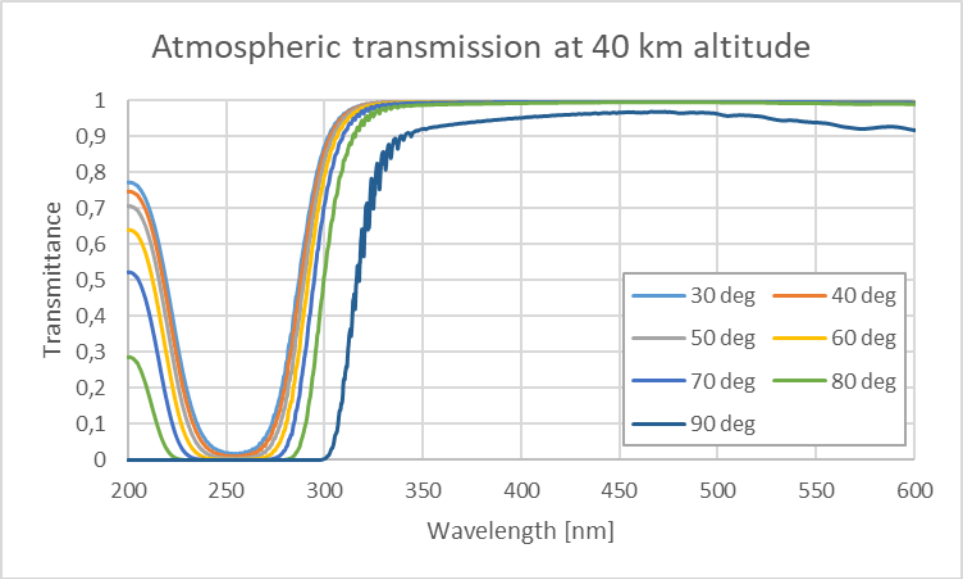

Figure 4: MODTRAN4 results for transmission at 40 km altitude

The plots clearly show a significant increase of the observable wavelength range with increasing flight altitude, particularly over the range from 200 nm to approx. 290 nm. A significant part only becomes observable at altitudes of around 38 km and higher. Transmittance at 200 nm also increases from approx. 28 % to almost 80 % (at 30° zenith angle) when increasing altitude from 30 km to 40 km.

Additionally, the plots show the significant impact of the zenith angle of observations on the atmospheric transmittance. Transmittance suffers considerably once observing at lower than approx. 60°.

Eventually, the quality of atmospheric transmission is dependent on the combination of flight altitude and zenith angle. For individual missions, the exact requirements on minimum

flight altitude and maximum zenith angle will differ, depending on the required sensitivity and on the exact spectral interval of interest. Generally, it can be noted, however, that:

- UV observations benefit from each km higher in flight altitude, with conditions becoming rather good over the 180-330 nm spectral range at approx. 38 km.
- Even at high flight altitudes, observations at large zenith angles are likely not recommendable. Transmittance starts to drop dramatically at zenith angles larger than approx. 60°.

4.1.2 Seasonal Effect on UV transmission

As mentioned above, at the considered UV wavelengths, atmospheric ozone is the main absorber. As Figure 5 and Figure 6 illustrate, the total atmospheric ozone column differs considerably over the year, but also over the globe (the figures are based on 2017 data from the OMI instrument on the Aura satellite). The displayed times of year were chosen to represent the spring and autumn turnaround conditions windows. While closer to the equator, such as over Alice Springs, the differences are not so drastic (yet somewhat better during local autumn), they are very noticeable for the higher and lower latitude sites, i.e. Kiruna, Timmins, and Wanaka.

In the case of Kiruna, the total ozone column in the spring window is at ca. 400 DU (Dobson Units), it decreases to ca. 300 DU by late summer. Figure 7 exemplarily shows the resulting change in atmospheric transmission for a flight altitude of 38 km and at two different zenith angles for Kiruna.[9]

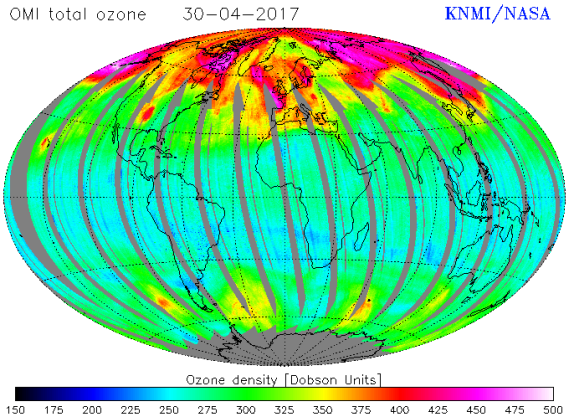

Figure 5: Global total ozone column on 30 April 2017

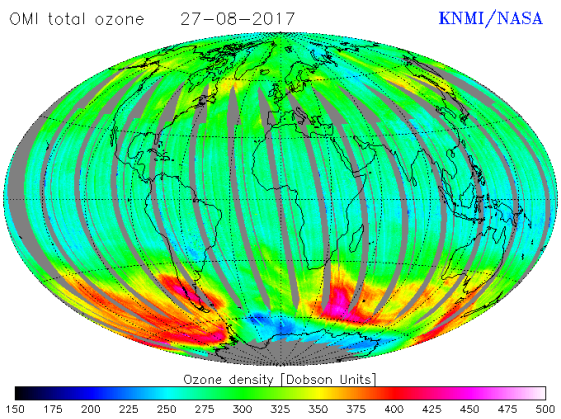

Figure 6: Global total ozone column on 27 August 2017

[9] These calculations do not take into account changes in the vertical distribution of ozone (or other atmospheric constituents) in between the two launch windows, but only the difference in total ozone columns.

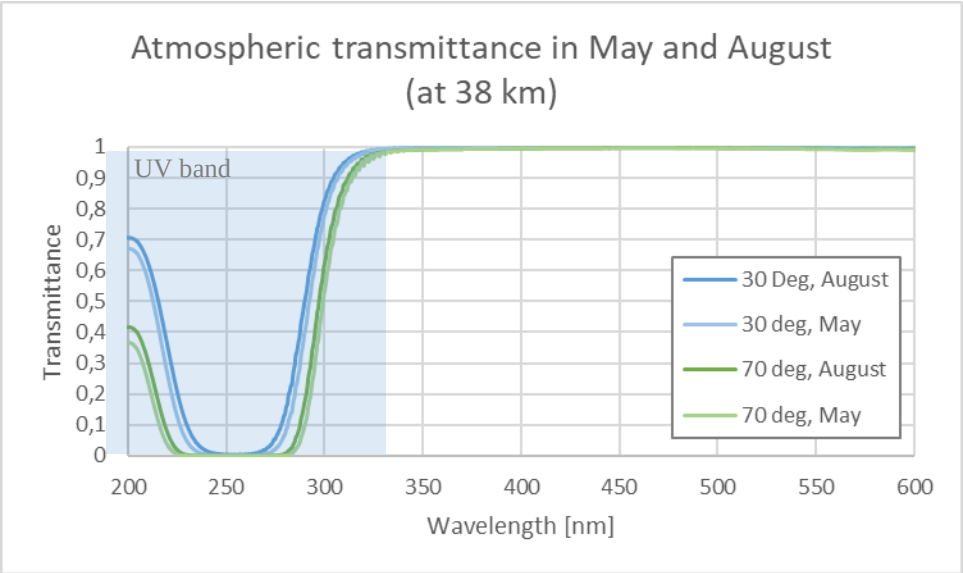

Figure 7: Difference in estimated atmospheric transmission at 38 km altitude over Kiruna for the two flight windows in end April/early May and late August (UV instrument measurement window: 180 to 330 nm)

These considerations clearly show that for the Kiruna and Timmins launch locations, if the choice exists, flights during the autumn turnaround conditions (August/September) are preferable over the spring turnaround conditions. For the Alice Springs launch location, flights during the local autumn turnaround conditions (April) are also preferable.

For flights from Wanaka, with flight durations that may reach 100 days and more, the effect will likely close to average out.

4.2 NIR

4.2.1 Requirements on Flight Altitude

The science cases underlying the conceptual design for the NIR flight platform as described in [RD11] emphasize observations of features at different wavelengths within the common range from 0.2 to 5 µm. At a closer look it turns out that the different wavelengths of interest pose rather different requirements on the minimum flight altitude of a balloon telescope.

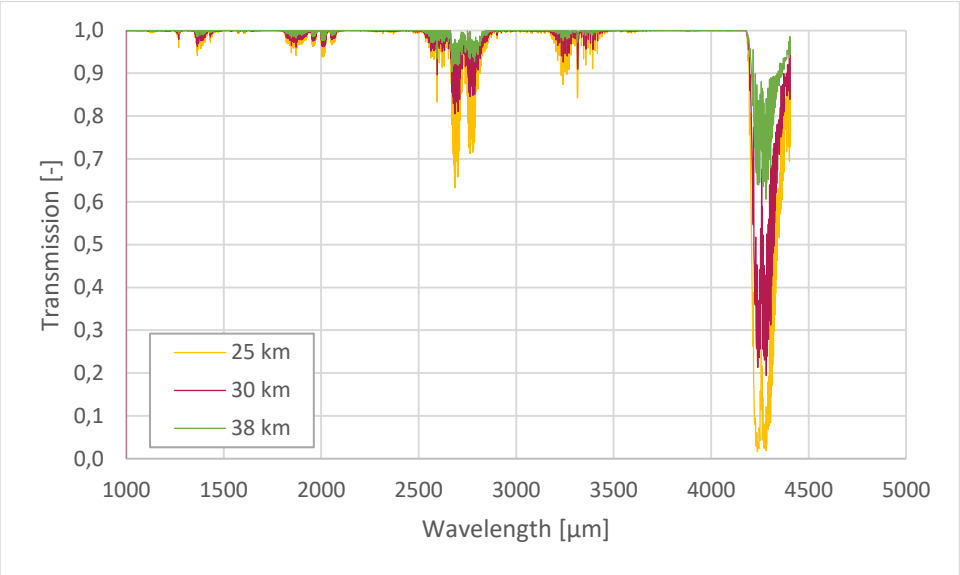

Figure 8: Atmospheric transmission over the wavelength range from 1 to 4.4 µm for different balloon flight altitudes. Data source: MODTRAN simulations. All data for zenith angles of 30°.

Figure 8 shows the atmospheric transmission at different balloon flight altitudes to illustrate this point.

The NIR observational needs of the science case on accretion in Young Stellar Objects (YSOs), which call for observations of the Paschen, Brackett, and Pfund series of hydrogen emission lines, already find reasonably good transmission at the relevant wavelengths. For the NIR observational needs of this science case, a flight altitude of 25 km would likely already suffice.

For exoplanet atmospheric observations as well as spectroscopic observations of small solar system bodies, however, the required flight altitude very much depends on the species desired to observe. Spectral lines of several interesting species are located at wavelengths that are already mostly unobstructed at 25 km, including H_2O, CO, CH_4, and NH_3. Particularly the CO_2 feature, however, falls into the spectral range around 2.25 µm, which still suffers strong absorption down to 25 km. For these observations, a flight altitude close to 40 km thus would certainly be desirable.

The intermediate conclusion at this point thus is that to fulfil all the science needs listed in [RD11], a flight altitude of 38 km or more is required for the NIR flight platform. This conclusion is, however, pending more detailed sensitivity calculations, also taking into account telescope and instrument details as well as background radiation.

4.2.2 Day vs. Night Observations

The NIR platform, with its science goal of covering the wavelength range from the UV to 5 µm in the NIR, falls into a technically interesting wavelength range. Within this range, the sky background emissions in the stratosphere reach the same strength during day and night time, so that from a certain point on, from a sky background perspective, it hardly matters anymore whether observations are performed during day or night. Additionally, within this wavelength range the thermal emission of the mirrors can be expected to replace the sky background as the dominating background source. In order to obtain a better impression of the relative influence of these three sources (day time sky background, night time sky

background, and mirror thermal emission), Figure 9 compares them over the wavelength range from 200 nm to 5000 nm.

It becomes obvious that above around 3 µm, the sky background does not differ anymore between day and night. Already earlier, however, at around 2.5 µm, mirror thermal emissions become the dominating background source, even surpassing the day time sky brightness (assuming a mirror temperature of -30°C, which is, given experience from past missions, a reasonable assumption for the temperature at night). Given the dominance of the mirror emission above 2.5 µm, the choice of day / night observations will only make a small difference above this wavelength. It can therefore be assumed that, from the perspective of average background brightness, it does not make a major difference whether observations are carried out during the day or during the night for wavelengths longer than 2.5 µm.

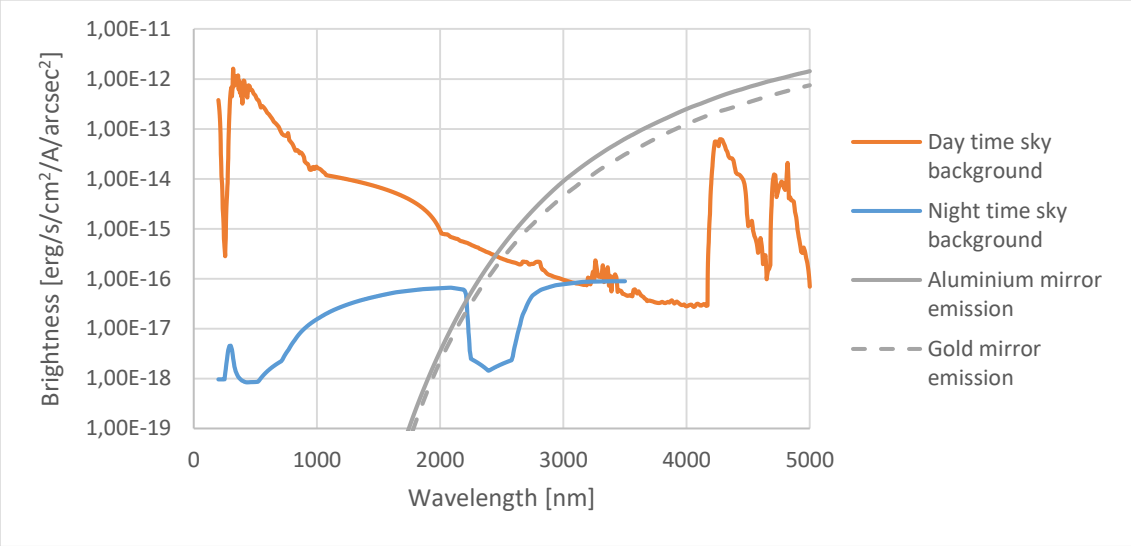

Figure 9: Comparison of different background sources for observations at 40 km altitude. Daytime sky background based on MODTRAN simulations (data from [RD1] & [RD2]). Nighttime sky background from THISBE measurements [RD3]. For comparison: thermal emissions from the primary mirror at 243 K, once coated with UV-enhanced aluminium, once with gold[10].

4.3 FIR

4.3.1 Requirements on Observational Conditions / Flight Altitude

In order to assess the technical requirement on the minimum flight altitude for FIR observations further, detailed calculations on the atmospheric transmission at wavelengths of interest were carried out for different assumed flight altitudes.

For this analysis, a residual content of precipitable water vapor (PWV) in the atmosphere above the observatory had to be assumed. For this purpose, different sets of PWV data at different locations (mostly dependent upon latitude) were analyzed. Table 2 shows the summary of this data. A location of particular interest was Antarctica, as, leaving super pressure balloons aside, the currently most promising location to perform long duration

[10] Based on past missions and thermal simulations, it can be optimistically assumed that the primary mirror can be passively cooled to as low as ~-30°C at night [RD4]. With some more effort in sun shielding, BLASTPol even managed to cool its primary to ~-20°C during daytime [RD5].

balloon flights is over Antarctica. Since, at least based on the small set of reviewed data, the Antarctic data also provides the highest PWV columns, these values were used for the analysis.

In addition to these literature values, Table 2 also mentions the PWV column as calculated by the radiative transfer code ATRAN [RD9], which is also used for atmospheric transmission and sensitivity calculations for observations from the airborne observatory SOFIA. This value is meant to provide a reference. For a detailed comparison of PWV values as resulting from the ATRAN model atmosphere with measured values, see [RD10].

Table 2: Summary of precipitable water vapour data

	PWV column [µm]				
Altitude [km]	**Antarctica[11]**	**0° N[12]**	**40° S**	**60° S**	**ATRAN**
30	n.a.	0.4	0.4	0.5	0.15
25	0.9	0.8	0.9	0.9	0.4
20	2.2	1.5	1.8	1.9	1.0
15	4.7	3.0	3.4	3.6	2.7
10	12.0	n.a.	n.a.	n.a.	
14 km reference					3.7

The calculations presented in the following were carried out with ATRAN using the PWV values for Antarctica, with the exception of 30 km altitude, where 0.5 µm were used, and the 14 km reference case, for which 3.7 µm were used (i.e. not using the PWV data from the ATRAN model atmosphere, which was more optimistic than the measured data).

All calculations were furthermore conducted for a zenith angle of 30°.

4.3.1.1 Wideband transmission over entire wavelength range

Firstly, a general comparison of the atmospheric transmissivity over the entire considered FIR spectral range from 30 to 200 µm was carried out. For this analysis, a spectral bin size of 1 µm was used.

As Figure 10 shows several wavelength regions exist where transmissivity drastically decreased for altitudes of less than 20 or 25 km. For a flight altitude of 25 km, at least the averaged transmissivity remains above 60 % over the entire spectral range. For 29 km flight altitude it even remains above 80 % for almost the entire spectral range.

[11] From [RD6], based on exemplarily H_2O mixing ratio measurements by sounding balloon over Syowa station, 26 November 2013. Underlying data from [RD7].

[12] Calculated based on H_2O mixing ratios (annual averages) collected by the Halogen Occultation Experiment (HALOE) on the Upper Atmosphere Research Satellite (UARS) [RD8].

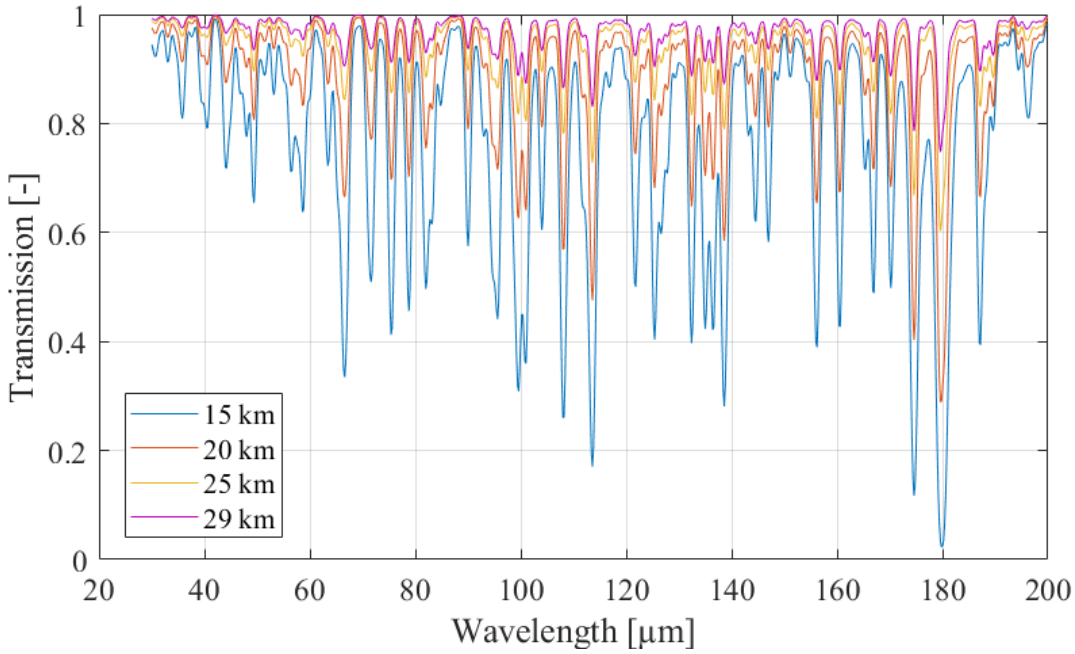

Figure 10: Comparison of broadband transmission over the considered spectral range from 30 µm to 200 µm

4.3.1.2 High spectral resolution transmission for interesting spectral lines

Information on wideband transmission only provides limited information for observations of particular spectral lines. For this reason, additional analyses were carried out for a selected set of emission lines identified as scientifically promising or relevant over the next decades (also see [RD11]). These calculations were carried out for a very high spectral resolution of 0.0001 µm (corresponding to R = 10^5 at 100 µm). Line widths were mostly chosen at 100 km/s.

Table 3 to Table 5 show the averaged transmission over their line widths for a selection of these species and lines.

Table 3: Average transmission at different altitudes for basic atomic and molecular emission lines

			Average transmission [-]			
Species / Line	**Wavelength [µm][13]**	**Line width (100 km/s) [µm]**	**14 km**	**20 km**	**25 km**	**29 km**
HD	58.770	0.04	0.09	0.58	0.90	0.96
[OI]	63.185	0.04	0.89	0.98	0.99	1.00
[NII]	121.8	0.08	0.03	0.36	0.79	0.92
[CII]	157.74	0.1	0.96	1.00	1.00	1.00

[13] Rest wavelength in µm

Table 4: Average transmission at different altitudes for emission lines of selected light hydrides

			Average transmission [-]			
Species / Line	**Wavelength [µm][14]**	**Line width (100 km/s) [µm]**	**14 km**	**20 km**	**25 km**	**29 km**
H_3O^+	181.054	0.12	0.27	0.57	0.79	0.88
H_3O^+	100.869	0.07	0.001	0.12	0.51	0.73
CH^+	179.62	0.12	0	0.003	0.18	0.45
CH^+	90.03	0.06	0	0.05	0.41	0.66
HF	121.697	0.08	0	0.03	0.24	0.41
HF	81.215	0.05	0.16	0.48	0.73	0.83

Table 5: Average transmission at different altitudes for emission wavelengths of different molecular ices

			Average transmission [-]			
Species / Line	**Wavelength [µm][15]**	**Line width [µm][16]**	**14 km**	**20 km**	**25 km**	**29 km**
H_2O	44.1	0.1	0.78	0.94	0.99	0.99
H_2O	45.7	0.1	0.99	1.00	1.00	1.00
H_2O	62.5	0.1	0.98	1.00	1.00	1.00
CO_2	85.5	0.1	0.97	0.99	1.00	1.00
CO_2	144.9	0.1	0.88	0.97	0.99	1.00
CH_3OH	33.0	0.1	0.49	0.70	0.85	0.90
CH_3OH	56.5	0.1	0.86	0.97	0.99	1.00

It should be noted at this point that the advantage of a balloon observatory compared with an airplane-based observatory with regard to the observation of molecular ices does not lie in the improved atmospheric transmission alone. The information in Table 5 is mostly provided at this point for the sake of completeness.

The information provided in Table 3 and Table 4 shows, however, that there is already a dramatic improvement in transmissivity for several lines in between 14 and 20 km flight altitude. Several others, e.g. the CH^+ line at 179.62 µm, only become worthwhile to observe closer to 25 km flight altitude. While there is still an increase in transmissivity of 10 to 50 % when moving from a flight altitude of 25 km to 29 km, the transmissivity values mostly look

[14] Rest wavelength in µm

[15] Rest wavelength in µm

[16] Assumed

promising already for a flight altitude of 25 km. For some species, it might even be worthwhile to observe from less than 25 km.

5 OBSERVATIONS PERFORMANCE POTENTIAL OF DIFFERENT FLIGHT ROUTES AND BALLOON TYPES

Different flight routes offer a considerably different sets of advantages and disadvantages for astronomical balloon flights. Short flight routes, which mostly take place over or not too far from the launch site, offer considerably easier logistics as compared to longer flight route and are therefore particularly well suited for test or checkout flights. Also the longer flight routes (and the times of year available to such flights) have considerably different implications on logistics and possible observations. Affected aspects include:

- Parts of the sky accessible for observations
- Total observation time available
- Time available for observations under night time conditions (if required)
- Atmospheric concentration of relevant absorbing gases (e.g. ozone)
- Logistical effort required for launch and flight preparation
- Ease of payload recovery
- Available daylight conditions for solar panel power supply
- Thermal variations over the flight time affecting lifting gas loss and potentially instrument sensitivities.

Super Pressure Balloons (SPBs), which we consider as one of the key technological innovations to increase the efficiency of balloon-based astronomical observations provide a new quality of advantages in several of the abovementioned aspects:

- They allow flight times and therefore scientific observation times more than twice as long as the ones possible at the moment;
- They allow ease in operations and flight routes with simpler logistics (i.e. not over the Arctic or Antarctica);
- They solve the challenge of thermal variations causing the need for massive ballast drops – therefore making long flights with day-night-shifts possible which combine the needs for night time observations and the need for sunlight for power supply.

These differences between the available flight routes shall be illustrated in more detail in the following sections, with a focus on the scientifically most relevant aspects of available observation time and access to the sky.

5.1 AVAILABLE OBSERVATION TIMES

Available observation times depend both upon the flight duration, the requirements posed by the type of observation (particularly whether nighttime observations are required), and thereby also on the geographical location. The requirements for the three different flight platforms (see also [RD12]) are shortly summarized below:

- UV/Vis flight platform: night time required (sun $\geq 6°$ below the horizon)

- NIR platform: night time required (sun ≥ 6° below the horizon[17])
- FIR platform: night time not required

In the following, to avoid confusion, the times in between civil dusk and civil dawn (i.e. when the sun is ≥ 6° below the horizon) are referred to as "dark times". Before reaching conclusions about the available observation times per flight platform and flight location / route, these dark times are illustrated for several locations.

5.1.1 Short Duration Flights

Dark times for Kiruna, Sweden (summer turnaround conditions)

Flight times: between 10 and 60 h

Flight period: second half of August

Latitude: 68° N

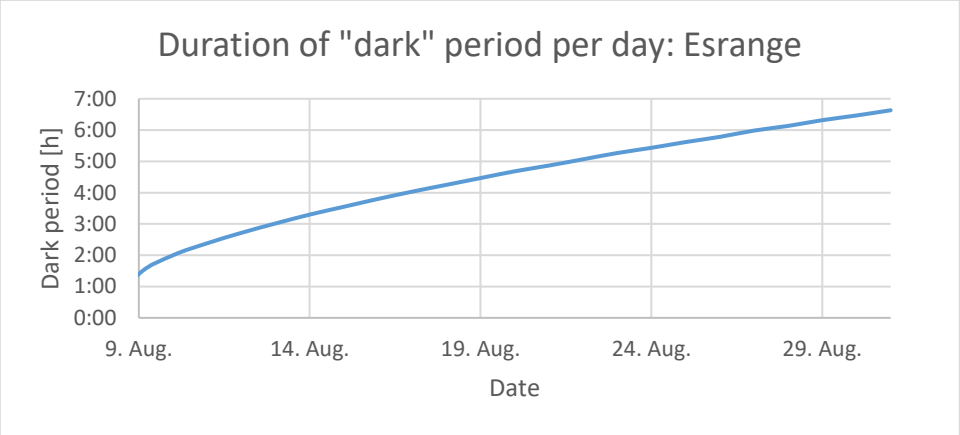

Figure 11: Duration of dark period per day over Esrange, Kiruna, during the time of summer turnaround conditions for 2021

One option for short duration flights is using the turnaround conditions of the stratospheric winds during late spring or late summer. A preliminary analysis showed that for UV observations, the window in late summer is much better suited due to the seasonally lower ozone content of the atmosphere, which is one of the major absorbers of UV light [RD13]. Therefore, only this period is illustrated in detail.

As a first possible location for flights during turnaround conditions, Esrange Space Center, close to Kiruna, Sweden, is considered. Figure 11 shows the duration of the number of dark hours per day during the time window of the summer turnaround conditions. It becomes rather clear that, due to the high latitude of the site, the dark times in late summer are still quite short.

Since for Esrange fortunately detailed statistics on possible flight times per day are available over the last several years, a more detailed analysis could also be carried out. This analysis was based on simulated flights under the wind conditions in the last several years, which

[17] Detailed analysis still outstanding

returned a flight time for each analyzed launch date. Based on the average of these flight times over the last three years, combined with data on the dark time per day, the "dark" observation time per flight that would have been available for different launch dates was calculated. As the nights become longer later in the year, this analysis was extended until the end of September. Figure 12 graphically illustrates the outcome of this analysis. As it shows, there are basically two periods during which long "dark" observation times can be achieved: either during the classical turnaround conditions during the second half of August, hoping for flight times that span several nights. Or in mid-September, when the nights are already longer, but available flight times shorter. In any case, the available "dark" observation time per flight adds up to about 8-10 h.

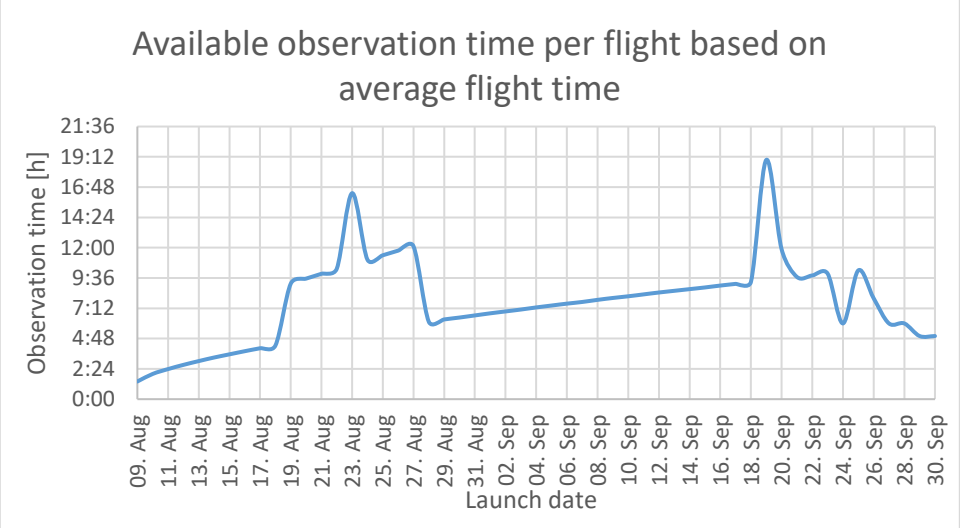

Figure 12: Available observation time for the UV/Vis platform over Kiruna depending on the launch date during the summer turnaround conditions (based on average simulated flight times in the years 2016-2018 and sun conditions for the year 2021).

<u>Dark times for Timmins, Canada (summer turnaround conditions)</u>

Flight times: up to ca. 35 h (currently, operational restriction)

Flight period: September

Latitude: 48° N

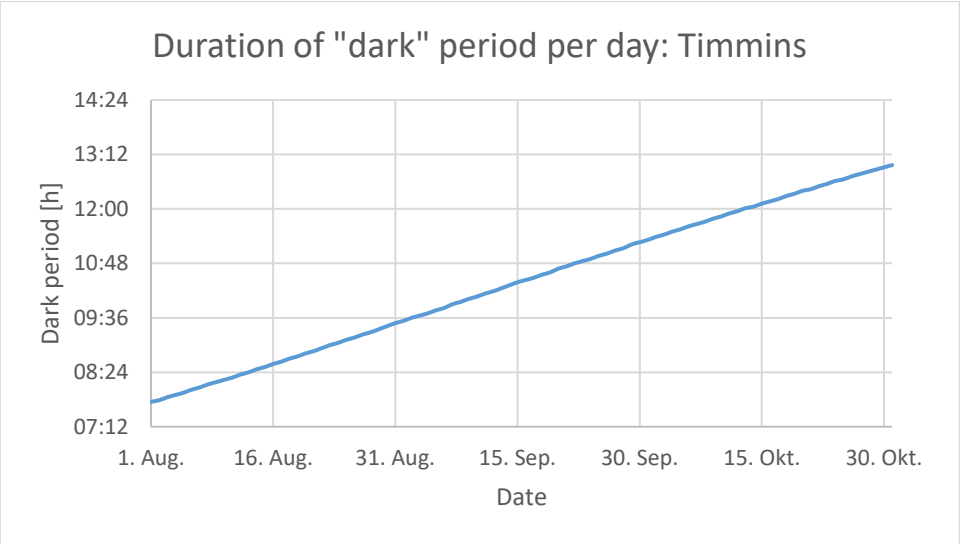

Figure 13: Duration of dark period per day over Timmins, Canada, during the time of summer turnaround conditions for 2021

Another option for using the summer turnaround conditions would be flying from the Timmins Stratospheric Balloon Based in Timmins, Canada. The base is located at lower latitudes than Esrange, i.e. nights in late summer are longer. In addition, the turnaround conditions at lower latitudes occur slightly in the year, which also favors longer nights times.

As Figure 13 illustrates, the dark period per day during September, which is the most suitable time for the turnaround conditions, is in between 10 to 11 h. The expected flight times of up to ca. 35 h might also allow for up to 20 h of observation time if two nights can be covered during one flight, more detailed analysis has not been carried out yet, however.

5.1.2 Long Duration (LDB) Flights

Dark times for Kiruna, Sweden (transatlantic flights during summer)

Flight times: up to 6 days

Flight period: late May to mid-August

Latitude: 68° N

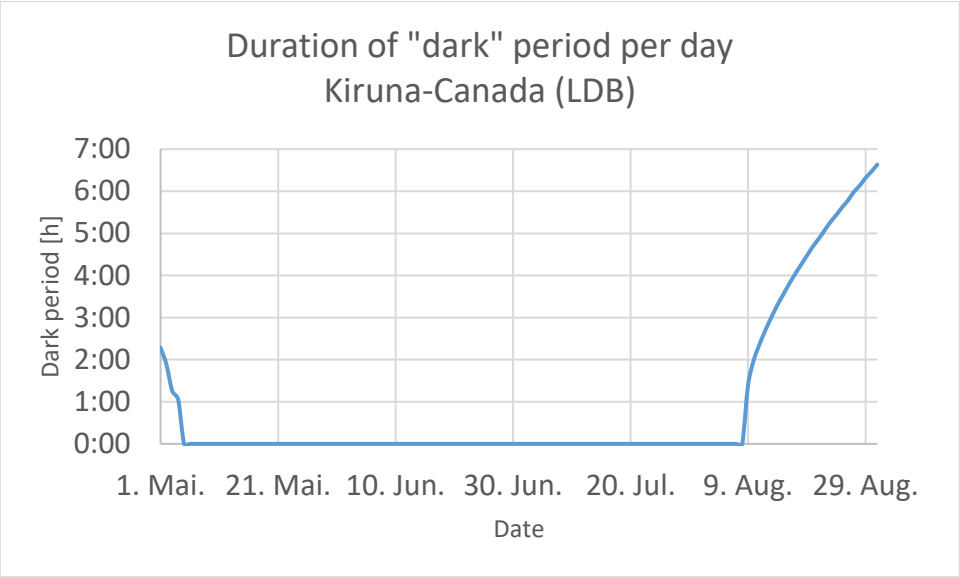

Figure 14: Duration of dark period per day at 68° N for transatlantic flights

For longer flights, one option on the Northern hemisphere are transatlantic flights. These flights are typically carried out in easterly winds during Northern summer, launching from Kiruna and landing in Canada. As Figure 14 indicates, this flight route provides reasonably stable thermal conditions, but little to no suitable observation time for observations that require night conditions.

Dark times for Antarctica (McMurdo, circumpolar flights during summer)

Flight times: typically 21 days, up to 55 days

Flight period: 01 December to 10 January

Latitude: 78° S

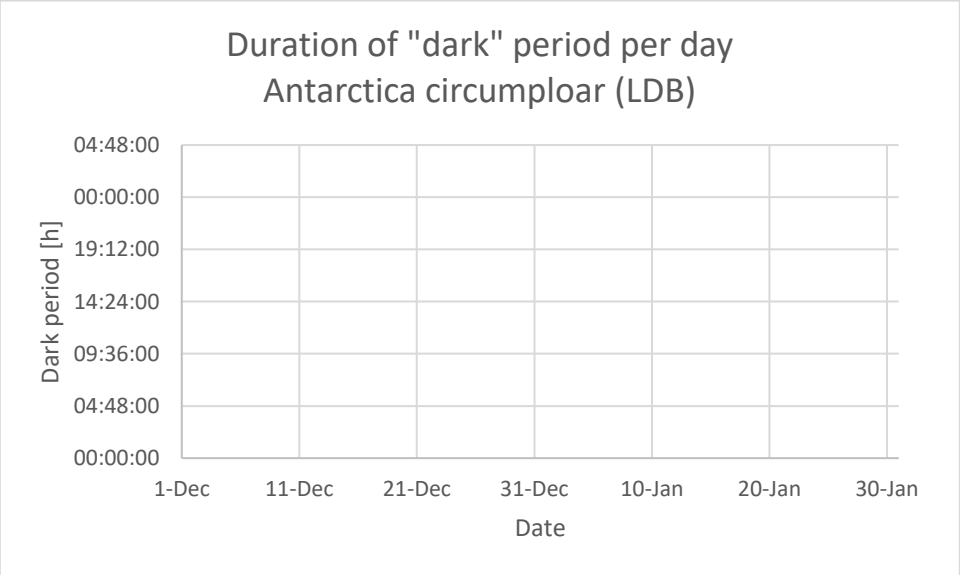

Figure 15: Duration of dark period per day at 78° S for Antarctic flights during Antarctic summer

The second common option for long duration flights is flying on circumpolar trajectories around the South pole (full circumpolar trajectories around the North pole are currently not possible due to missing overflight permissions over Russia). These flights are typically carried out from the McMurdo base, where considerable supporting infrastructure exists. Due to weather conditions (and the availability of sun for power supply), flights are carried out during Antarctic summer. While the Antarctic summer, with the sun constantly above the horizon, provides reasonably stable thermal conditions and constant solar power supply, as Figure 15 indicates, no dark observation times are available at all.

5.1.3 Ultra Long Duration Flights (ULDB)

Dark times for Southern mid-latitudes (Wanaka, New Zealand, circumglobal flights)

Flight times: achieved 46/54 days[18], goal of 100+ days

Flight period: 25 March – 08 September

Latitude: 45° S

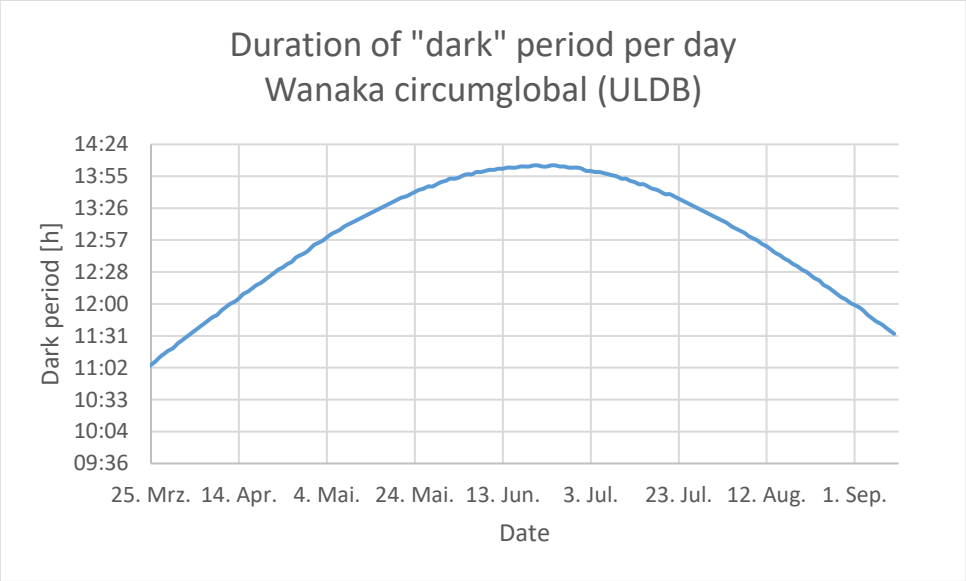

Figure 16: Duration of dark period per day at 45° S for circumglobal ULDB flights

Figure 16 eventually shows the available dark observation times per day for the currently used flight route for Ultra Long Duration flights with SPBs. The assumed launch window for these flights is March 25th to May 31st [RD14]. Assuming that the goal of 100 days of flight will be achieved in the near future, this leads to a flight window until September 8th. It should be noted that, due to the day-night cycles on this route, long flight times at these latitudes are only achievable with SPBs. In comparison with the polar flight routes, mid-latitude routes feature changing thermal environment and require energy storage to provide power during night times.

[18] 46 days with a 5000 lbs suspended mass balloon in 2016, 54 days with a 1500 lbs suspended mass balloon in 2008

5.1.4 Summary

Table 6 summarizes the expected achievable observation times for the different flight routes mentioned above.

Table 6: Summary of achievable observation times on different flight routes

	Pessimistic estimate		**Optimistic estimate**	
	Dark times [h][19]	**Total obs. time [h][20]**	**Dark times [h][19]**	**Total obs. Time [h][20]**
Short duration flights				
Kiruna	9.5	15	12	40
Timmins	10	n.a.	20	35
Long duration flights				
Kiruna - Canada	0 - 6.5	100	0 - 6.5	120
Antarctica	0	400	0	1050
Ultra long duration flights				
Wanaka circumglobal	683	1000	1350	2000

These estimates are based on the following assumptions:

- Kiruna, short duration:
  - Pessimistic estimate: flight in mid-September, i.e. comparably short flight time but long night
  - Optimistic estimate: flight in second half of August, i.e. long flight time, but short nights
- Timmins, short duration:
  - Pessimistic estimate: one night
  - Optimistic estimate: two nights, total flight time limited to ~35 h due line-of-sight ground support
- Kiruna, long duration flights:
  - Pessimistic estimate: 5 days of flight, launch in between 01 May and 01 August
  - Optimistic estimate: 6 days of flight, launch see above
  - 6.5 h of dark time only apply for launch on 01 May
- Antarctica, long duration flights:
  - Pessimistic estimate: 21 days of flight
  - Optimistic estimate: 55 days of flight
- Wanaka, ultra long duration flights:
  - Pessimistic estimate: 50 days of flight, launch in between 25 March and 31 May
  - Optimistic estimate: 100 days of flight, launch see above

[19] With the sun ≥ 6° below the horizon (on ground)

[20] Assuming 20% service time unavailable for observations

- All long and ultra long duration flights:
    - For total observation time: 20 % of flight time assumed for housekeeping
    - For dark times: housekeeping is done during daytime, no overhead

5.2 SKY ACCESSIBILITY

In addition to the achievable observation times per flight, the accessible areas of the sky need to be taken into account. The most obvious limitation in this regard is the inaccessibility of the Southern / Northern sky for flights at high Northern or Southern latitudes respectively. Sections 5.2.1 to 5.2.3 illustrate these restrictions and the accessible areas of the sky for each flight route covered above.

All analyses of sky accessibility are based on the following assumptions:

- A minimum telescope elevation angle of 30° is required to keep airmass acceptable
- A maximum telescope elevation angle of 65° is imposed by the balloon obstructing the zenith
- Restrictions by potentially required sun or moon avoidance angles are disregarded at this point.

For more details on the analysis see [RD13].

5.2.1 Short duration flights

Kiruna, Sweden

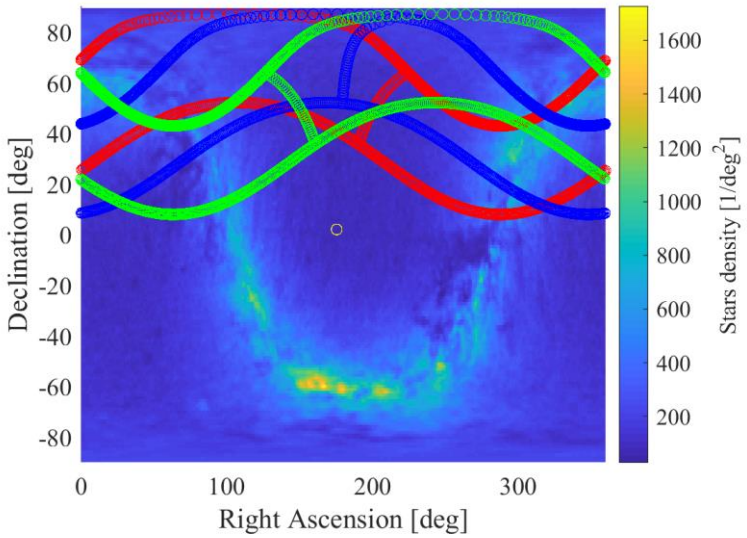

Figure 17: Accessible parts of the sky from Kiruna, Sweden (red: 20:00 CEST [18:00 UT], blue: 24:00 CEST [22:00 UT], green: 05:00 CEST [03:00 UT], yellow dot: sun on 2021-09-17)

Figure 17 shows the accessible parts of the sky from Kiruna, Sweden, as a snapshot on 2021-09-17. The different colored bands show the outer edges of the accessible sky areas at different times of day. The area within each band is accessible at the given time.

The background image is a density plot based on the Tycho-2 star catalogue. Clearly visible as a bright band is the Galactic plane, including the Galactic Center at ca. 266° RA, -29° Dec.

The plot shows that the observable area of the sky from Kiruna is limited to a declination of around 5 to 90°.

Timmins

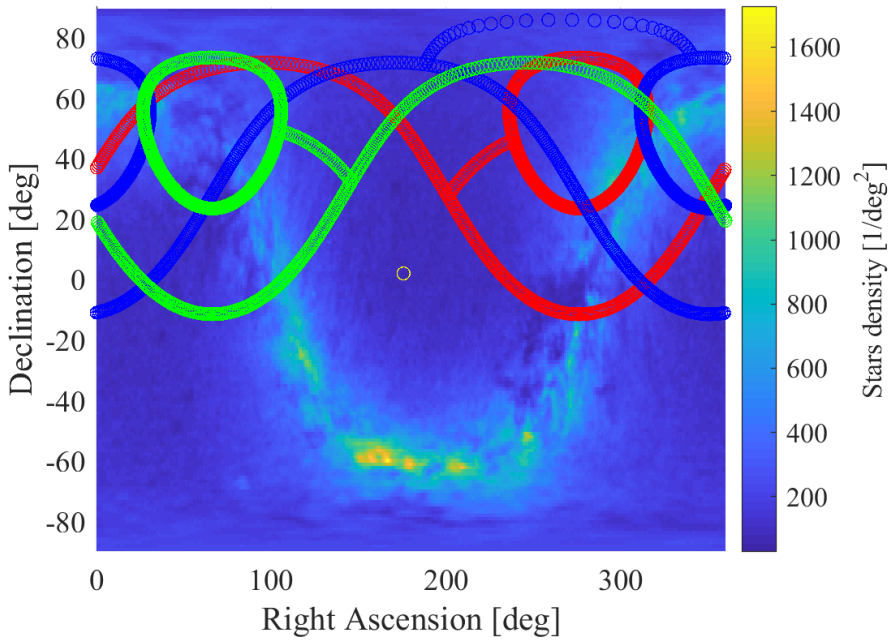

Figure 18: Accessible parts of the sky from Timmins, Canada (red: 20:00 EDT [24:00 UT], blue: 01:00 EDT [05:00 UT], green: 06:00 EDT [10:00 UT], yellow dot: sun on 2021-09-17)

Figure 18 shows the same information as Figure 17, only for flights over Timmins, Canada. The "encircled" areas with their centers at around 50° Declination mark the part of the sky obstructed by the balloon at the given time. The accessible area of the sky at a given time is therefore the area north of the lower colorful band, except of the area obstructed by the balloon.

The plot indicates that the accessible sky from Timmins is limited to declinations of about -10° and higher.

5.2.2 Long duration flights

Kiruna

Assuming that a floating balloon remains more or less at the same latitude during a transatlantic flight, the viewing conditions onto the sky are very similar to the ones from Kiruna. Therefore, for transatlantic flights from Kiruna, in good approximation the observable sky areas as depicted in Figure 17 apply.

Antarctica

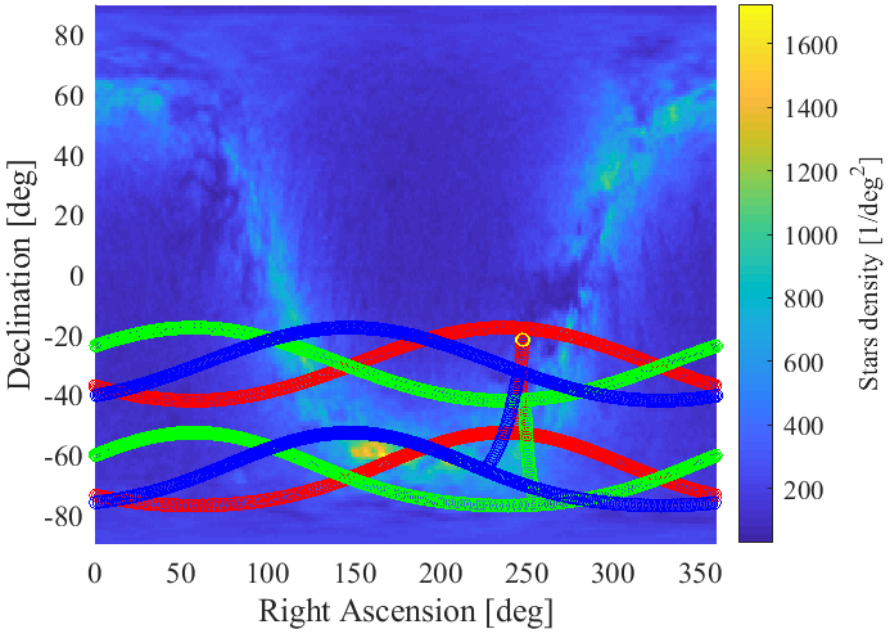

Figure 19: Accessible parts of the sky from McMurdo station, Antarctica (red: 13:00 NZDT [00:00 UT], green: 01:00 NZDT [12:00 UT], blue: 07:00 NZDT [18:00 UT], yellow dot: sun on 2021-12-01)

Figure 19 shows the accessible sky for flights from McMurdo over Antarctica, again assuming that the balloon will stay more or less at the same latitude throughout the flight. It is particularly noticeable that even in the beginning of December, the sun is within the observable area for around 1/3rd of the day. It should also be noted that the sun's distance to the Galactic Center during this time of year reaches a minimum of slightly more than 5° around Dec. 18th.

The plot furthermore shows that the Southern celestial pole is not visible on the Antarctic flight route due to the obstruction of the balloon towards the zenith. Including the Southern celestial pole would require an increase of the max. observable elevation angle to 77°, which, with a 5° angular separation between the telescope line of sight and the balloon would require a flight train length of 380 m. This is not considered realistic.

Assuming a flight of 50 days duration and a launch on December 1st, the area as illustrated in Figure 20. Other launch dates within the flight window show only minor changes. Due to the low latitude of the flight route, it is obvious that observations at declinations higher than

ca. -15° degree are not possible, at least when requiring a minimum elevation angle of 30° to limit the airmass for observations.

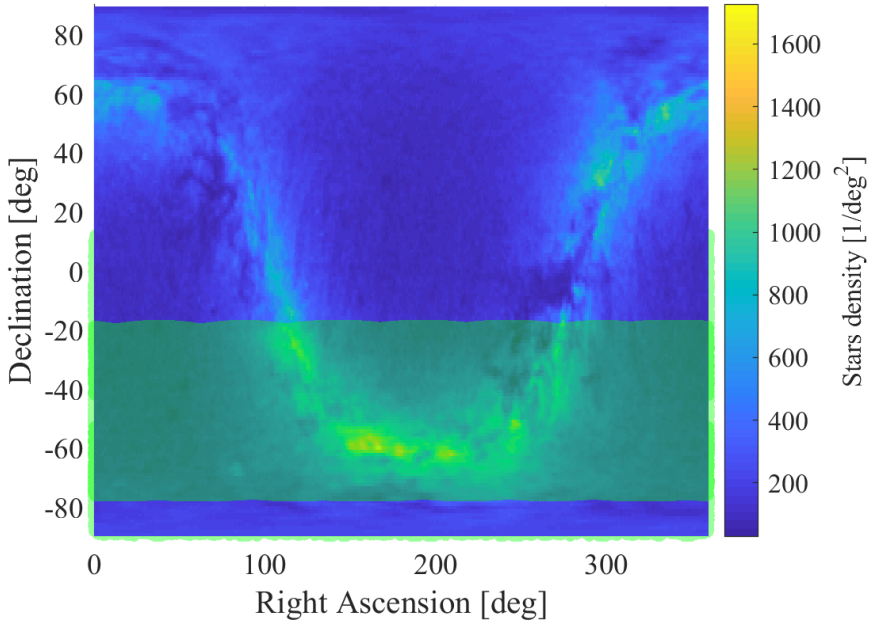

Figure 20: Accessible area of the sky from McMurdo station, Antarctica over the timeframe from 2021-12-01 to 2022-01-20 (constraints: minimum elevation 30°, maximum elevation 65°).

In order to provide an indication of which areas would become accessible if lower elevation angles were allowed, i.e. higher airmass and therefore atmospheric absorption was tolerated, Figure 21 provides the accessible sky for minimum required elevation angles of 10° and 0°.[21] These analyses show that, if observations can actually be carried out at elevations as low as 0°, at a maximum objects with around 13° declination can be observed.

[21] Due to the flight altitude, the minimum possible elevation of targets still observable, assuming no obstacles on the horizon, would actually be approx. -5.5°. Due to the possibility of obstacles on the horizon, this is not a good reference case, however.

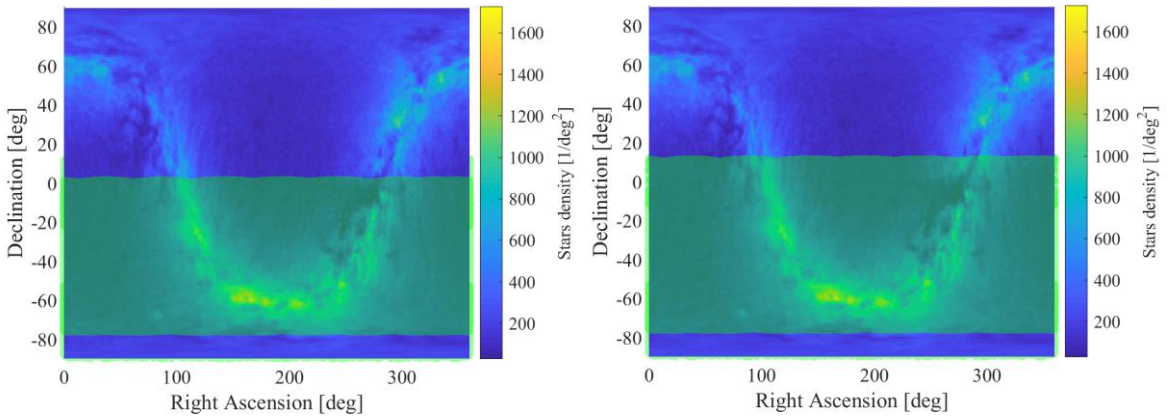

Figure 21: Accessible sky from McMurdo in case of a minimal elevation constraint of 10° (left) and of 0° (right)

Arctic flights (launching from Svalbard)

An interesting flight option, particularly in combination with circumpolar Antarctic long duration flights, would be circumpolar flights around the North Pole. These could complement the Antarctic flights with access to the Northern celestial hemisphere. A potentially suitable launch site for Northern circumpolar flights would be Svalbard (Norway), which has been used for launches of large astronomical balloons in the past (particularly for the OLIMPO mission). While full circumpolar flights around the North Pole are currently politically not possible due to missing overflight rights, it might be worth working towards a political solution. Figure 22 shows the area of the sky accessible during a 50 day flight from Svalbard.

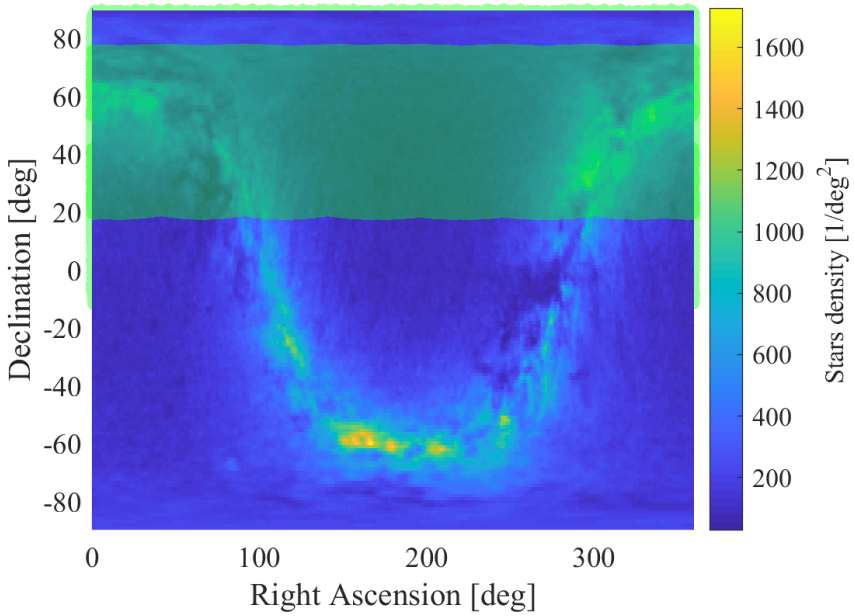

Figure 22: Accessible area of the sky from Svalbard, Norway, over the timeframe from 2021-06-01 to 2021-07-20 (constraints: minimum elevation 30°, maximum elevation 65°).

Figure 20 and Figure 22 make it obvious that with the minimum elevation constraint of 30°, not the entire sky can be covered by a combination of circumpolar flights from McMurdo and from Svalbard. If observations were acceptable down to 12° elevation, however, coverage of almost the entire sky (except at the celestial poles) would be possible with a combination of these two flights (see Figure 23).

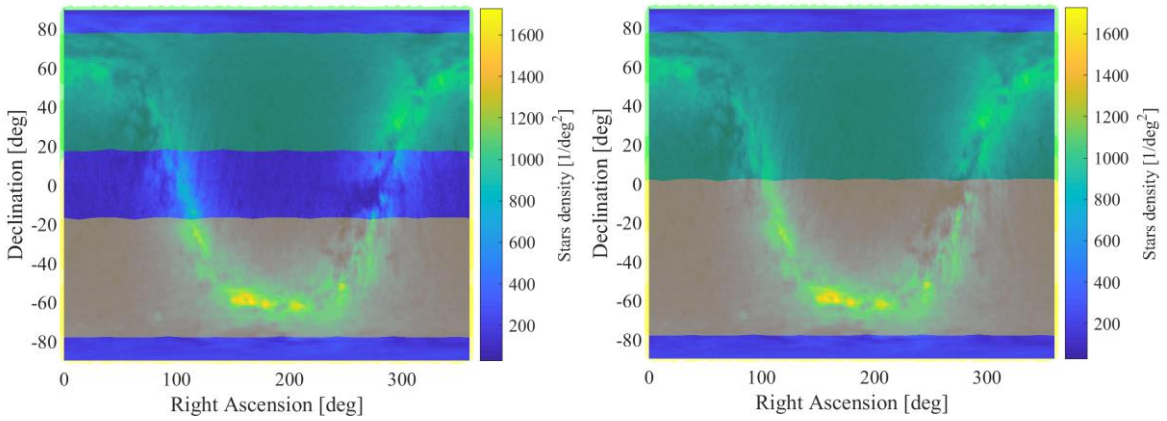

Figure 23: Accessible area of the sky using a combination of Northern and Southern circumpolar flights. Left: with a minimum elevation constraint of 30°. Right: with a minimum elevation constraint of 12°. Green shaded area shows accessibility from Svalbard, yellow shaded area shows accessibility from McMurdo (each for a 50 days flight)

5.2.3 Ultra long duration flights

Southern mid latitudes (Wanaka, New Zealand)

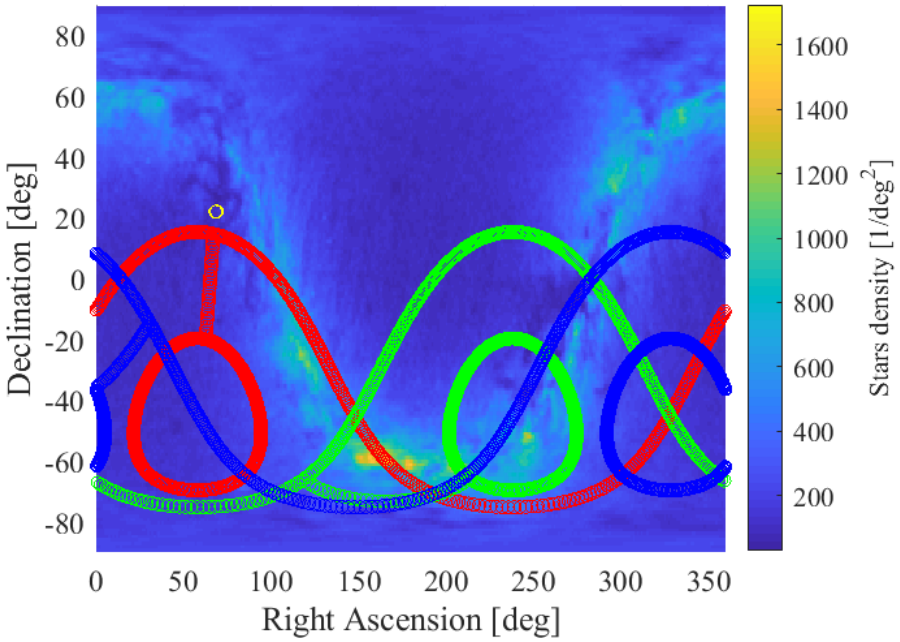

Figure 24: Accessible parts of the sky from Wanaka, New Zealand (red: 12:00 NZST [00:00 UT], green: 00:00 NZST [12:00 UT], blue: 06:00 NZST [18:00 UT], yellow dot: sun on 2021-05-31)

Figure 24 shows the accessible areas of the sky during a circumglobal ULDB flight launch from Wanaka, again assuming that the balloon remains roughly at the same latitude throughout the flight.

5.2.4 Summary

To summarize the analysis of the observable sky, Table 7 shows the limitations on the observable sky for the different flight routes. The limitations are expressed in minimum and maximum observable declination.

The illustrations underline the differences between high- and mid-latitude flight routes. High-latitude flight routes allow continuous access to smaller parts of the sky for extended amounts of time (for 14 h and more, partly for > 24 h). Mid-latitude routes on the other hand offer access to larger portions of the sky, but for shorter continuous times (up to ~ 8.5 h, depending on the declination). Only for the regions around the celestial pole (above ca. 75° declination) mid-latitude routes offer continuous access.

The suitability of the flight routes therefore depends to a large degree on the targeted scientific application.

Table 7: Summary of limitations on the observable sky for different flight routes (for observable elevation angles between 30° and 65°)

	Observable sky declination	
	Min.	**Max.**
Short duration flights		
Kiruna	8°	87°
Timmins	-11°	90°
Long duration flights		
Kiruna – Canada	8°	87°
Antarctica	-77°	-18°
Ultra long duration flights		
Wanaka circumglobal	-90°	15°

6 DESIGN DETAILS/ASSUMPTIONS FOR CONCEPTS

This chapter describes details and assumptions underlying the technical design for the concepts as described in the Preliminary Technical Specification [RD12]. The focus is thereby set on mass and design drivers, which particularly include the telescope and the power supply systems.

Instrument assumptions and design details of all other subsystems will be described in more detail in the ESBO *DS* Conceptual Design Report.

6.1 UV/VIS (SMALL) FLIGHT PLATFORM

The UV/VIS flight platform practically coincides with the ESBO *DS* prototype platform. In order to avoid duplication, a detailed technical description of this platform is omitted at this point as it will be described in detail in D10.2, D11.1, and D11.2.

6.2 NIR (MEDIUM-SIZED) PLATFORM

6.2.1 Telescope Mass Estimate

1-m aperture class telescopes are commonly available commercially, tailored for ground-based use. A flight-worthy telescope will require mechanical adaptations, careful athermal structural design, and an optical design optimized for the specific application. We can, however, use the existing and available telescopes for a first mass estimate for the flight system. For this estimate, we use the (slightly updated) list of telescopes provided in [RD16] and extrapolate to a primary aperture diameter of 1 m using a fitted power function (see Figure 25).

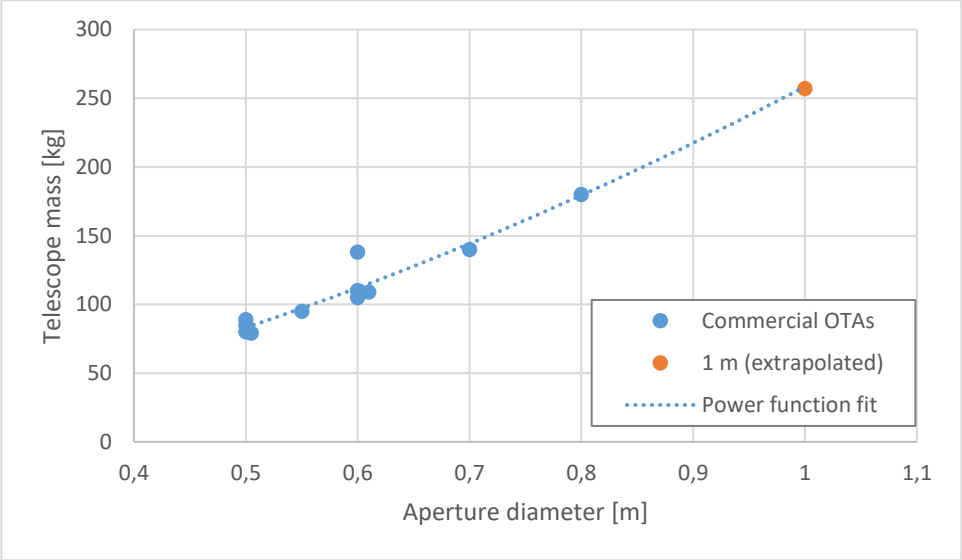

Figure 25: Full telescope mass (full Optical Tube Assembly, without mount) of commercially available telescopes (data mostly from [RD16])

This leads to an estimated mass of approx. 256 kg for the full telescope. This is considerably heavier than lightweighted space telescopes of comparable size, e.g. ARIEL with an estimate of 126 kg for a 1.1 m x 0.73 m aperture telescope [RD18], and is considered a reasonable conservative estimate.

6.2.2 Power System Sizing

6.2.2.1 General Assumptions

Some general assumptions are made for the sizing of the power system for all following cases. Firstly, a breakdown of the day into the operating modes listed in Table 8 is assumed. This breakdown is assumed to apply for both daytime and nighttime (in the case of mid-latitude circumglobal flights).

Table 8: Breakdown of operating modes

Scientific observation	80 %
Re-positioning	10 %
Service / Checkup	10 %

Secondly, the efficiencies as listed in Table 9 were used, assuming multicrystalline, single-junction Si solar cells.

Table 9: Assumed solar array efficiencies

Power distribution efficiency (solar arrays through batteries to loads) [RD15]	0.6	
Power distribution efficiency (directly from solar arrays to loads) [RD15]	0.8	
Solar array efficiency [RD16]	20%	
Solar array Fill Factor [RD16]	80%	
Efficiency due to non-optimal temperature of arrays [RD15]	80%	
Efficiency due to change in vertical angle over course of 1 day[22]	0.92	
Efficiency due to other angular misalignment (no pointed arrays) [RD17]	0.9	
Solar constant	1366	W/m^2
Total power generation capability	145	W/m^2

And thirdly, the technical parameters as listed in Table 10 were used for the sizing of secondary batteries, assuming Lithium Ion batteries.

Table 10: Lithium Ion secondary batteries technical parameters

Specific energy [RD16]	200 Wh/kg
Max. depth of discharge	90 %

6.2.2.2 Environmental Conditions for circumglobal flights at mid-latitudes

Table 11 lists the sun elevation angle ranges along with the geometric solar panel efficiencies for the circumglobal flight window at mid-latitudes from Wanaka, NZ. The optimized solar panel angle in this case is 16°, the lowest daily average geometric efficiency, which is used for the solar panel sizing, is around 92 %.

[22] Number for geometrical efficiency applies for mid-latitudes flights, as does the total power generation capability calculated with it. For the geometrical efficiency for Antarctic flights, see section 6.2.2.3.

Table 11: Range of sun elevation angles at 45° South latitude during ULDB flight period and geometric solar panel efficiencies for an elevation angle of the solar panel normal vector of 16°

	Sun elevation [°]		Sun vector to solar panels normal [°]		Geometric efficiency of solar panels [-]		
	Min elev.	Max elev.	at sun min. elev.	at sun max. elev.	at sun min. elev.	at sun max. elev.	Avg.
Mar 25th	0	44.7	16	28.7	0.9612617	0.87714616	0.91920393
Apr 25th	0	33.3	16	17.3	0.9612617	0.9547608	0.95801125
May 25th	0	25.5	16	9.5	0.9612617	0.9862856	0.97377365
June 25th	0	23.1	16	7.1	0.9612617	0.99233194	0.97679682
July 25th	0	26.9	16	10.9	0.9612617	0.98195871	0.9716102
Aug 25th	0	35.7	16	19.7	0.9612617	0.94147054	0.95136612
Sept 8th	0	40.8	16	24.8	0.9612617	0.90777748	0.93451959
						Overall average	0.95504022

For the mid-latitude flights, a distinction between night- and daytime operations needs to be made. The (from a power perspective) worst case scenario is 14 h of night time and 10 h of daytime in June / July (see section 5.1.3), which is used for the power system sizing. As the night time is also valuable scientific observation time, the same split-up of operating modes as detailed in Table 8 is used as the first assumption.

Table 12: Power modes and energy consumption per day for mid-latitude ULDB flights

	Power Modes				
	Launch + Ascent	Observation	Re-Positioning	Service/Checkup	
Total avg. power	134.83	388.18	146.33	148,53	W
System margin	30%	30%	30%	30%	
Total avg. Power incl. Margin:	175.28	504.63	190.23	193.09	W
Total duration of phase:	3	19.2	2.4	2,4	h
Total req. energy:	404.49	190.229	351.192	356.472	Wh
Total duration of phase during day:		8	1	1	h
Total req. Energy during day:		4037.072	190.229	193.089	Wh
Total duration of phase during night:		11.2	1.4	1.4	h
Total req. Energy during night:		5651.9008	266.3206	270.3246	Wh

With the efficiencies as listed in Table 9, the battery characteristics as stated in Table 10 and an assumed area specific mass of the solar cells of 1.5 kg/m^2 [RD17], this leads to an estimated mass of the solar panels of 22 kg and an estimated mass of the batteries of 65 kg.

6.2.2.3 Environmental Conditions in Antarctica

All conceptual designs assume non-pointing solar arrays installed at an optimized elevation angle to account for the sun's movement over the day. In order to determine the optimal angle as well as the maximum loss in efficiency due to non-optimal orientation of the solar arrays towards the sun, the sun's position over the potential flight time has to be taken into account. Table 13 lists the corresponding sun elevation angles as well as the resulting geometric solar panel efficiencies for the optimized solar panel angle of 21° (elevation angle of solar panel normal). The lowest daily average geometric efficiency, which is used for the solar panel sizing, is around 97 %.

Table 13: Range of sun elevation angles over Antarctica during LDB flight period and geometric solar panel efficiencies for an elevation angle of the solar panel normal vector of 21°

	Sun elevation [°]		Sun vector to solar panels normal [°]		Geometric efficiency of solar panels [-]		
	Min elev.	Max elev.	at sun min. elev.	at sun max. elev.	at sun min. elev.	at sun max. elev.	Avg.
Nov 1st	2	26.5	19	5.5	0.94551858	0.9953962	0.97045739
Nov 15th	6	30.6	15	9.6	0.96592583	0.98599604	0.97596093
Dec 1st	10	33.9	11	12.9	0.98162718	0.97476119	0.97819419
Dec 15th	11	35.4	10	14.4	0.98480775	0.96858316	0.97669546
Jan 1st	11	35.2	10	14.2	0.98480775	0.96944535	0.97712655
Jan 15th	9	33.4	12	12.4	0.9781476	0.97667228	0.97740994
Feb 1st	5	29	16	8	0.9612617	0.99026807	0.97576488
						Overall average	0.97594419

Since the sun is always over the horizon during Antarctic flights, no split-up of the operation (and power consumption) in night- and daytime operation needs to be done. Instead, the sizing of batteries and solar arrays is done based on the assumption that observations might require worst possible pointing (90° away from the sun) for 3 h a day, and that the energy required for this time must be recharged within a day. All calculations are based on the power modes and assumed energy consumptions thereof listed in Table 14.

Table 14: Power modes and energy consumption per day for Antarctic flights

	Power Modes				
	Launch + Ascent	Observation, day	Re-Positioning	Service/Checkup	
Total avg. power	134.83	388.18	146.33	148.53	W
System margin	30%	30%	30%	30%	
Total avg. Power incl. Margin:	175.28	504.63	190.23	193.09	W
Total duration of phase:	3	19.2	2.4	2.4	h
Total req. energy:	404.49	7453.056	351.192	356.472	Wh

With the efficiencies as listed in Table 9, the battery characteristics as stated in Table 10 and an assumed area specific mass of the solar cells of 1.5 kg/m^2 [RD17], this leads to an estimated mass of the solar panels of 8 kg and an estimated mass of the batteries of 14 kg.

6.2.3 Structure Mass Estimate

The structural mass is estimated based on the structural mass fraction of past scientific ballooning gondolas as analyzed in [RD16], set to 12% for an assumed carbon fibre composite structure.

Given the yet unknown structural implications of a soft landing system, traditional (honeycomb) crash pads were assumed in addition to the guided parafoil system. Their mass was calculated based on [RD19], conservatively assuming a gondola dry mass of 2300 kg and a maximum allowable landing acceleration of 5 to 10 g at a vertical landing velocity of 10 m/s (which is assumed to be considerably above that reachable with a guided parafoil).

6.2.4 Attitude Determination and Control System Estimate

The pointing system is assumed as a two-stage system, with a coarse outer system and an image stabilization system as part of the optical system. The outer system again is assumed to employ a single reaction wheel for azimuthal control and motors acting on the telescope for elevation control. The main mass driver of this system is the reaction wheel, which is estimated following the design guideline to provide 1:20 of the moment of inertia of the full gondola.

6.3 FIR (LARGE) PLATFORM

6.3.1 Mirror Mass

The large primary mirror required on the FIR platform to fulfill the angular resolution requirement will be one of the mass drivers of this flight platform. In order to estimate the mass for the primary, a number of legacy missions were regarded.

A lot of effort has been put into light weighting mirrors in the past years, particularly for space and balloon missions, but also for fast ground-based telescope (e.g. for Space Situational Awareness purposes). Instead of the more conventional Zerodur, four main materials are used for lightweight mirrors:

- Aluminium (high coefficient of thermal expansion, CTE)
- Berrylium (very expensive, mainly used on space missions)
- Silicon Carbide (SiC)
- Carbon Fibre Reinforced Polymer (CFRP)

Figure 26 shows the achieved areal mass density of primary mirrors for space and balloon missions built with these materials (it should be noted that SPICA and CALISTO are only concepts, whereas the other mirrors were realized and flew).

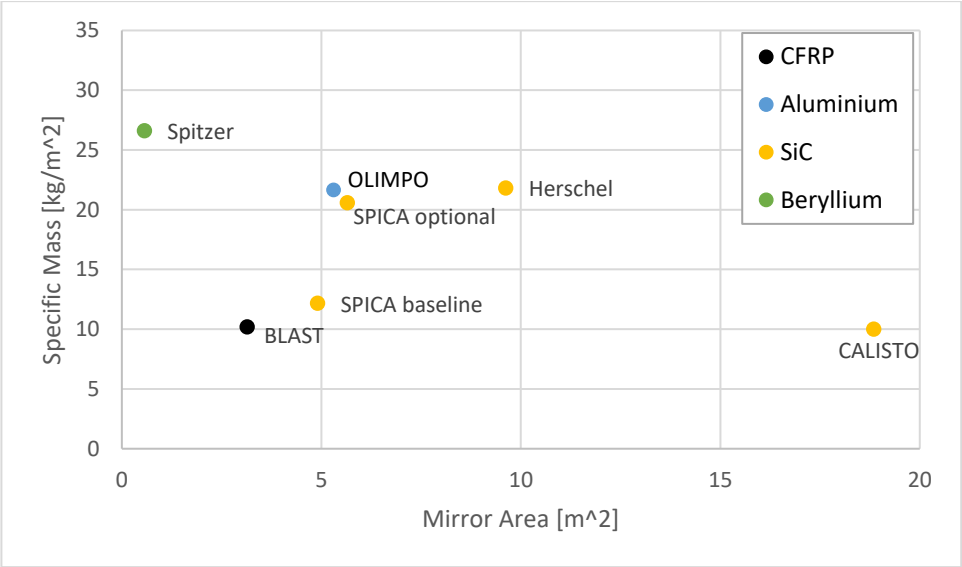

Figure 26: Specific mirror mass of FIR space and balloon telescopes

Due to the very low mass, the very low CTE, and comparatively high flexibility in manufacturing different shapes, CFRP was chosen for further analysis for the FIR platform.

For the first analysis, a classical Cassegrain layout of the telescope was assumed. For this layout, two different mirror shapes were considered: a full circular mirror of 5 m aperture diameter, and a mirror with an elliptical aperture with a major axis of 5 m and a minor axis of 2.5 m. Table 15 shows the estimated mass of the mirror for both shapes and for different assumed areal densities. We assume that, with the current improvements to CFRP mirrors, areal densities of 20 kg/m^2 can be reached even for larger mirrors (the areal density of the 2 m diameter BLAST mirror is around 10.2 kg/m^2). Since an elliptical aperture shape will pose more stability issues than a circular one, we conservatively estimate that we can reach an areal density with the elliptical aperture mirror of 30 kg/m^2, which leads to a mirror mass of around 300 kg.

A full circular mirror, assuming the same areal density, would have a mass of ~590 kg, which, considering first mass budget estimates (see [RD12]), does not appear to be feasible with current balloons. In order to reach a similar mass as the elliptical aperture mirror, a circular one would need to have an areal density of around 15 kg/m^2. While this appears challenging, lower areal densities have been reached for the BLAST mirror and for a CFRP test mirror for Herschel.

We therefore assume a circular mirror for the first concept, while we give the topic further careful consideration under WP5 (Conceptual Design, see also section 7.1.2).

Table 15: Total primary mirror mass for different assumed areal densities

	5 x 2.5 m elliptical	**5 m circular**
Aperture Area	9.8 m^2	19.6 m^2
Mass (30 kg/m^2)	295 kg	590 kg
Mass (21.8 kg/m^2)	214 kg	429 kg
Mass (15 kg/m^2)	147 kg	295 kg

6.3.2 Full Telescope Mass

To estimate the rest of the telescope mass (structure + secondary mirror), we again consider similar telescopes and past missions. We expect space based telescopes to require a somewhat lighter telescope structure, as the structures do not have to withstand deformations due to changing gravitational loads. As Figure 27 indicates, this holds true for Herschel when comparing it to balloon-borne and ground-based telescopes.

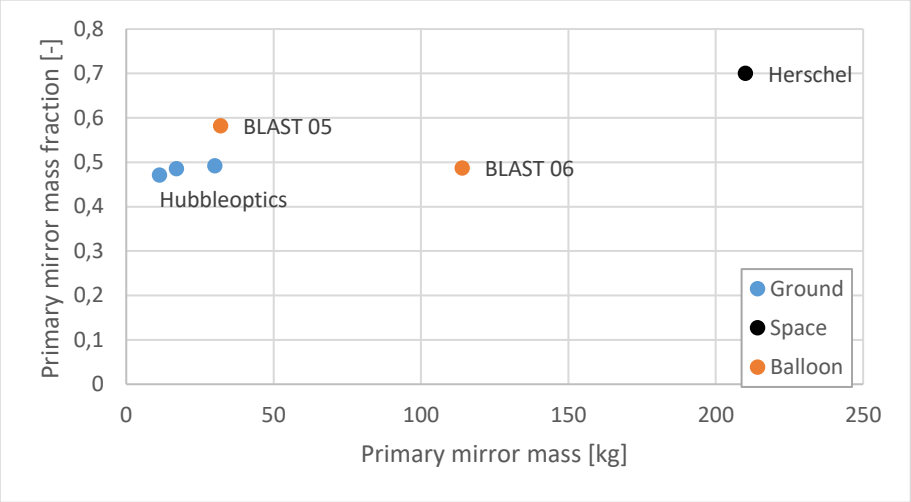

Figure 27: Primary mirror mass as a fraction of the total telescope mass (including structure & M2) for different balloon-borne, space-borne, and ground based telescopes (three differently sized telescopes between 0.4 and 0.6 m primary diameter from the company Hubbleoptics)

Taking the balloon-borne and ground based telescopes as examples, a primary mirror fraction of 0.5 of the total telescope mass appears reasonable and will be assumed for the further concept estimates.

6.3.3 Power System Sizing

6.3.3.1 General Assumptions

For the power system sizing of the FIR platform, the same general assumptions in terms of breakdown of operation modes over a day, solar array efficiencies, and secondary battery characteristics apply as for the NIR platform (and listed in section 6.2.2.1).

6.3.3.2 Power System Sizing for Antarctic Flights

As Antarctic flights of the FIR platform would be carried out at the same time of year as those of the NIR platform, the environmental conditions (particularly the sun elevation angles) would be the same as those listed in section 6.2.2.3. We consequently also use an optimized solar panel angle of 21° (elevation angle of solar panel normal) and a worst-case elevation efficiency of 97 %.

Since the sun is always over the horizon during Antarctic flights, no split-up of the operation (and power consumption) in night- and daytime operation needs to be done. Instead, the sizing of batteries and solar arrays is done based on the assumption that observations might require worst possible pointing (90° away from the sun) for 5 h a day, and that the energy required for this time must be recharged within a day. All calculations are based on the power modes and assumed energy consumptions thereof listed in Table 16.

Table 16: Power modes and energy consumption per day for Antarctic flights

	Power Modes				
	Launch + Ascent	Observation, day	Re-Positioning	Service/Checkup	
Total avg. power	134.83	2188.18	146.33	148.53	W
System margin	30%	30%	30%	30%	
Total avg. Power incl. Margin:	175.28	2844.63	190.23	193.09	W
Total duration of phase:	3	19.2	2.4	2.4	h
Total req. energy:	404.49	42013.056	351.192	356.472	Wh

With the efficiencies as listed in Table 9, the battery characteristics as stated in Table 10 and an assumed area specific mass of the solar cells of 1.5 kg/m^2 [RD17], this leads to an estimated mass of the solar panels of 36 kg and an estimated mass of the batteries of 148 kg.

6.3.3.3 Power System Sizing for circumglobal flights at mid-latitudes

As circumglobal flights of the FIR platform would be carried out at the same time of year as those of the NIR platform, the environmental conditions (particularly the sun elevation angles) would be the same as those listed in section 6.2.2.2. We consequently also use an optimized solar panel angle of 16° (elevation angle of solar panel normal) and a worst-case elevation efficiency of 92 %.

For the mid-latitude flights, a distinction between night- and daytime operations needs to be made. The (from a power perspective) worst case scenario is 14 h of night time and 10 h of daytime in June / July (see section 5.1.3), which is used for the power system sizing. As the night time is also valuable scientific observation time, the same split-up of operating modes as detailed in Table 8 is used as the first assumption.

Table 17: Power modes and energy consumption per day for mid-latitude ULDB flights

	Power Modes				
	Launch + Ascent	Observation	Re-Positioning	Service/Checkup	
Total avg. power	134.83	2188.18	146.33	148.53	W
System margin	30%	30%	30%	30%	
Total avg. Power incl. Margin:	175.28	2844.63	190.23	193.09	W
Total duration of phase:	3	19.2	2.4	2,4	h
Total req. energy:	404.49	42013.056	351.192	356.472	Wh
Total duration of phase during day:		8	1	1	h
Total req. Energy during day:		22757.072	190.229	193.089	Wh
Total duration of phase during night:		11.2	1.4	1.4	h
Total req. Energy during night:		31859.9008	266.3206	270.3246	Wh

With the efficiencies as listed in Table 9, the battery characteristics as stated in Table 10 and an assumed area specific mass of the solar cells of 1.5 kg/m^2 [RD17], this leads to an estimated mass of the solar panels of 95 kg and an estimated mass of the batteries of 260 kg.

6.3.4 Structure Mass Estimate

The structural mass is estimated based on the structural mass fraction of past scientific ballooning gondolas as analyzed in [RD16], set to 12% for an assumed carbon fibre composite structure.

Given the yet unknown structural implications of a soft landing system, traditional (honeycomb) crash pads were assumed in addition to the guided parafoil system. Their mass was calculated based on [RD19], conservatively assuming a gondola dry mass of 2300 kg and a maximum allowable landing acceleration of 5 to 10 g at a vertical landing velocity of 10 m/s (which is assumed to be considerably above that reachable with a guided parafoil).

6.3.5 Attitude Determination and Control System Estimate

The pointing system is assumed as a two-stage system, with a coarse outer system and an image stabilization system as part of the optical system. The outer system again is assumed to employ a single reaction wheel for azimuthal control and motors acting on the telescope for elevation control. The main mass driver of this system is the reaction wheel, which is estimated following the design guideline to provide 1:20 of the moment of inertia of the full gondola.

7 TRADE-OFFS

This chapter provides details on trade-offs carried out during the early design of the different concepts. On the one hand, it therefore provides justification and reasoning for some of the choices made. On the other hand, some of these choices will need to be reviewed and either confirmed or revised during the conceptual design under WP5.

Particularly with regard to the FIR platform, the downscoping options to meet the SPB mass envelope (section 7.1.1) will need to be reviewed carefully from a scientific perspective.

The choice of mirror size and shape (elliptical vs. circular, section 7.1.2) will equally be reviewed under WP5 when investigating the design of large CFRP mirrors for the FIR in more detail.

7.1 FIR PLATFORM

7.1.1 Mass reduction for SPB flights

Table 18 shows the baseline mass budget of an FIR platform for SPB flights. SPBs require less ballast than ZPBs, therefore freeing up some useable for payload. However, current SPBs can also carry less suspended mass (5,500 lbs for NASA's 18.8 MCF balloon, as flown in 2017) and the mid-latitude trajectory increases battery and solar panel allocation in order to support the gondola during nighttime. As the table shows, this leads to the conclusion that the flight platform as conceptualized in section 5.4.1 of [RD12] (adapted to the needs of a ULDB flight) cannot be support by current SPBs.

An efficient option to reduce the mass would be reducing the payload mass, particularly the telescope mass, by decreasing the size of the telescope. However, this would mean a) decreasing the scientific performance and b) that the telescope design would need to be adapted to the flight route, if no major performance decrease on ZPB flight routes should be accepted.

Table 18: FIR flight platform for SPBs baseline mass budget

	Item mass (CBE) [kg]	# of items	Total CBE [kg]	With system margin [kg]
1. Payload				1184
1.1 Telescope			600	750
1.1.1 Primary Mirror			300	375
1.1.2 Structure + Secondary Mirror			300	375
1.2 Scientific Instrument			327	409
1.2.1 Heterodyne HEB Receiver			18	23
1.2.2 Spectrometer (8x 1GHz FFT analyzer)			9	11
1.2.3 Cryostat			300	375
Dry mass			125	156
Cryogen			175	219
1.3 Payload Electronics				0
1.4 Add-on instruments			20	25
2. Bus				1623
2.1 Attitude Determination & Control			179	224
2.2 Command & Data Handling			25	31
Balloon Service System			25	31
2.3 Communications & Tracking			29	36
LOS System			20	25
BLOS System			9	11
2.4 Electrical Power Subsystem			452	565
Batteries			338	423
Solar Panels			114	143
2.5 Thermal Control			20	25
2.6 Structures & Mechanisms			363	454
Gondola Structure			299	374
Crash Pads			64	80
2.7 Soft Landing System			230	288
3. Balloon Support Systems				3
3.1 Strobe Lights				0
3.2 Passive Radar Reflector				0
3.4 ATC transponder	1	2	2	3
3.5 Primary parachute				0
Suspended "dry" mass total				2810
Margin				-315

Maximum suspended mass	2495
Ballast mass assuming max. suspended mass	0
Max. suspended "dry mass"	2495

Alternatively, as several subsystems scale with time, observation time can be reduced to meet the current limitations. Two effective options exist:

- Reducing the duration of the flight, which particularly decreases the required cryogen mass (assuming that no closed-cycle cooler is used),
- Reducing the observation duty cycle (or, generally, the power consumption) during night time, which relaxes the requirements for the power system.

A rough estimation shows that the "cost" of mass reduction in terms of sacrificed observation hours is likely significantly less when reducing the observation duty cycle (about 2.3 h/kg, vs. 6.8 h/kg if reducing the flight duration), so that this approach is further considered.

Reducing the nightly duty cycle of observations from 80% to 28% would lead to sufficient mass saving in the power system to meet the mass restriction.

Assuming, however, that with sufficient progress in the development of large CFRP mirrors, similar areal densities to that of the Herschel (SiC) mirror can be reached, i.e. 22 kg/m^2, the nightly duty cycle would only need to be reduced to 60%.

Considering these two cases, and taking into account the night durations during the ULDB flight period as mentioned in section 5.1.3, the observation times as summarized in Table 19 would be available for FIR observations (given that these observations also can be carried out during daytime).

Table 19: Available FIR observation time in case of reduced nightly duty cycle (always assuming 80% duty cycle during daytime)

Nightly duty cycle	**Observation time (50 days flight)**	**Observation time (100 days flight)**
28 %	691 h	1374 h
60 %	857 h	1710 h

The resulting masses of the mass budget elements with this mass reduction strategy would be the following:

Table 20: Telescope & power system element masses for 22 kg/m^2 primary mirror areal density and 60 % observational duty cycle during night time

Mass of primary mirror	216 kg
Mass of telescope structure & secondary	216 kg
Mass of batteries	260 kg
Mass of solar panels	95 kg

Alternatively, one could also aim for technology developments that might relax the challenge. This particularly concerns the following areas[23]:

[23] These development needs are also listed in the Prototype Requirements Document. The respective codes are provided in brackets. The closed cycle-cooler development is listed under "enabling technologies" in [RD20].

1. SPBs with increased suspended mass capabilities (~ 3 t) (LT-DevN-ULDB-03)
2. Lightweight large (5 m aperture in one dimension) CFRP mirrors with areal densities of 22 kg/m^2 or less (already required for the abovementioned strategy) (LT-DevN-LWT-01)
3. Closed-cycle coolers for FIR instruments that make consumable coolants obsolete.

As a baseline, thus the adjustments according to Table 20 are used for the SPB FIR flight system concept, while the abovementioned technology developments are also included as enabling major improvements in [RD12].

7.1.2 Elliptical vs. circular mirrors

As already mentioned in section 6.3.1, the primary mirror is one of the expected mass drivers. Its size, however, also has a major influence on the observation performance in two aspects:

1) An elliptical mirror leads to an anisotropy of the angular resolution, with higher angular resolution in the direction of the major axis of the elliptical shape. This anisotropy can be eliminated by observing the same target at different telescope orientations. However, this would mean a decrease in observing efficiency and, depending on the flight trajectory, will not be possible for all targets on the sky without actively rotating the primary mirror.
2) A larger light collecting area (as a circular mirror would provide it) decreases required observation time to reach a particular signal to noise ratio and thereby increases observation efficiency.

The primary mirror therefore has been (and will be) given particularly close attention. As mentioned in section 7.1.2, CFRP was chosen as the most promising material. With a detailed design analysis of the mirror still to be done, it remained uncertain, however, which average areal density and therefore total mass of the primary mirror could be achieved. We therefore adopted an inverted approach, analyzing which areal density would be acceptable under the original preliminary mass allocations of 300 kg (without system margin). The acceptable areal density then was compared to that of existing mirrors.

Figure 28 summarizes the analysis, showing the total mirror mass over an assumed average areal density for both an elliptical and a circular mirror.

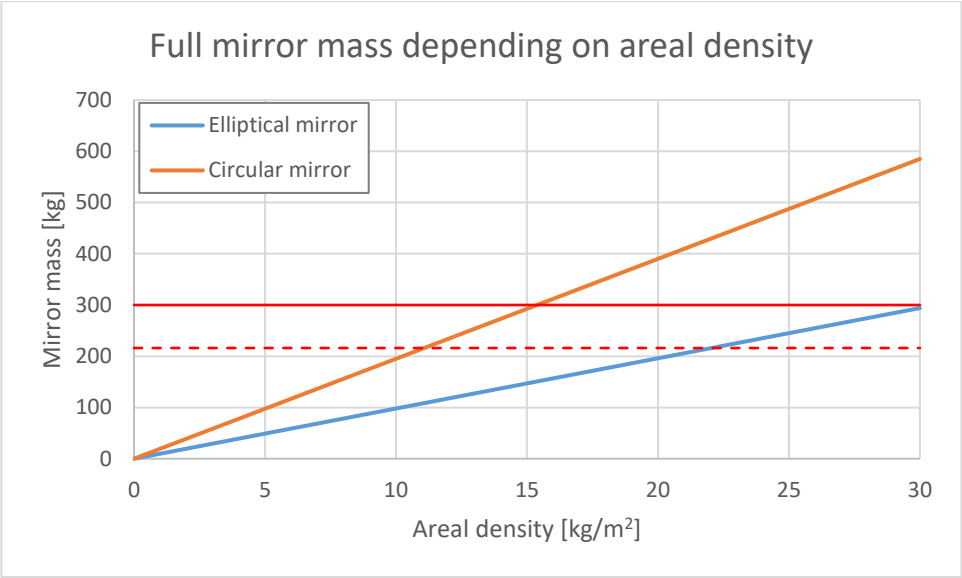

Figure 28: Comparison of full mirror mass depending on the achieved average areal density of the mirror, for both an elliptical mirror (total area: 9.8 m^2) and a full circular mirror (total area: 19.6 m^2). The solid red line indicates the original preliminary mass allocation of 300 kg, the dashed red line the possible mass reduction goal of 216 kg for SPB flights.

Optimistically estimating that an areal density of 15 kg/m^2 will be achievable for a large balloon mirror, the circular mirror was selected as the baseline at this point.